

Morphing the left atrium geometry: The role of the pulmonary veins on flow patterns and thrombus formation

Sergio Rodríguez-Aparicio^a, Conrado Ferrera^{a,b}, María Eugenia Fuentes-Cañamero^c, Javier García García^d and Jorge Dueñas-Pamplona^{d,*}

^aDepartamento de Ingeniería Mecánica, Energética y de los Materiales, Universidad de Extremadura, Avda.de Elvas s/n, Badajoz, 06006, Spain

^bInstituto de Computación Científica Avanzada (ICCAEX), Avda.de Elvas s/n, Badajoz, 06006, Spain

^cServicio de Cardiología, Hospital Universitario de Badajoz, Avda.de Elvas s/n, Badajoz, 06006, Spain

^dDepartamento de Ingeniería Energética, Universidad Politécnica de Madrid, Avda. de Ramiro de Maeztu 7, Madrid, 28040, Spain

ARTICLE INFO

Keywords:

atrial fibrillation
atrial morphing
flow split ratio
left atrial appendage
patient-specific modeling
pulmonary vein orientation
stagnant blood volume

ABSTRACT

Background: Although significant advances have been made in the field of computational fluid dynamics (CFD) to simulate the left atrium (LA) in atrial fibrillation (AF) conditions, the connection between atrial structure, flow dynamics, and blood stagnation in the left atrial appendage (LAA) remains unclear. Deepening our understanding of this connection would have important clinical implications, as the thrombi formed within the LAA are one of the main causes of stroke.

Aim: To highlight and better understand the fundamental role of the PV orientation in the formation of atrial flow patterns, and quantifying systematically its effect on blood stasis within the LAA.

Methods: Two patients with different types of atrial flow patterns were selected for the study. The atria were segmented and subsequently morphed to modify the PV orientation in a highly controlled manner. CFD analysis was performed using a kinematic model to reproduce AF conditions. Results were projected into the universal left atrial appendage coordinate (ULAAC) system to enhance data visualization and comparison.

Results: The position of the main atrial vortex, which governs the atrial flow patterns, is significantly influenced by variations in the PV orientation. Moreover, the flow split ratio affects how the position of the main atrial vortex influences the formation of a stagnant region within the LAA and, thus, the risk of stroke. These findings may have important clinical implications, as standard clinical practice does not take into account PV orientations, flow split ratio, or LA morphology when assessing stroke risk for a particular patient.

1. Introduction

Atrial fibrillation (AF) is the most common type of supraventricular arrhythmia [1]. In 2019, this disease affected 33.1 million people worldwide and caused 219.4 thousand deaths [2]. Its prevalence has increased by 33% in the past two decades, and this trend is expected to continue for the next three decades [3].

AF appears as a result of an alteration in the electrical impulses of the pulmonary veins (PV). As a consequence, atrial contraction becomes irregular [4]. This irregular contraction can last for a short period (paroxysmal AF) or become permanent (permanent AF). If this abnormal contractility persists, harmful remodeling processes can appear in the medium and long term, affecting both the biomechanical and electrical functions of the myocardium. These simultaneous processes lead to increased blood stasis in the left atrial appendage (LAA) [5].


The LAA is a lobe-like structure within the left atrium (LA), originated during embryonic atrial development [6, 7]. Its morphology is highly patient-specific [8], and in terms of its physiological function, it works as a contractile reservoir or as a decompression chamber depending on the phase of

the cardiac cycle [9]. Its contractility is impaired in patients with non-valvular AF and is the source of thrombus in up to 91% of these patients [7]. In fact, more than 3.5 million ischemic strokes are caused by thrombi formed in LA. LA is also believed to be the cause of other 30% ischemic strokes in patients with sinus rhythm or subclinical AF [10]. Therefore, patients with AF have a five-fold increased risk of stroke than those not affected by this disease [11, 7].

The electrical isolation of PV and the closure of LAA are standard treatments for AF [12, 1]. Closure of LAA is a common practice to prevent stroke in patients whose anticoagulant response is not satisfactory [12, 7]. However, there is a group of patients who have AF recurrence after electrical isolation [13] or device-related thrombus after LAA closure [14, 15]. Therefore, a deeper understanding of atrial flow patterns is required to develop new treatments.

Current imaging techniques, such as transesophageal echocardiography and 4D Magnetic Resonance Imaging, provide useful but limited flow information within the LAA [16, 17]. However, computational fluid dynamics (CFD) is a tool that allows the use of the computational power of machines to model fluid flow. Since its inception, when it was employed to analyze flow in simple geometries, it has evolved to explore flow patterns in complex geometries such as the heart. CFD models range from single LA or left ventricle (LV) models [18, 19, 20], to whole left heart

Corresponding author

 jorge.duenas.pamplona@upm.es (J. Dueñas-Pamplona)

ORCID(s): 0000-0001-7990-5969 (S. Rodríguez-Aparicio);

0000-0002-2274-1374 (.C. Ferrera); 0000-0002-6570-6624 (J.

Dueñas-Pamplona)

models [21, 22, 23]. Models can even integrate the fluid-structure interaction with electrophysiological or biomechanical mechanisms [22, 24, 25, 26].

LA hemodynamics analysis has drawn increasing attention due to the health problems mentioned above. Many recent studies have focused on the analysis of LAA stasis [19, 27, 28, 29, 30, 31, 24, 32, 33], which is known to be related to the risk of thrombosis in patients with AF. There is also clinical evidence on the relationship between LAA morphology and stroke risk in patients with AF [34, 35]. Therefore, the link between LAA stasis and LAA morphology has been thoroughly analyzed [29, 28, 32, 36] and new parameters have been introduced to quantify LAA stasis [30, 24, 37]. However, although different classifications have been proposed for LAA morphology [38, 39], a subjective component associated with the radiologist limits the reproducibility of these classifications. For that reason, other researchers have studied more specific variables within LAA such as volume, width, height, bending angles, tortuosity, ostium diameters, etc. [40, 41, 42, 43, 35, 44], or tried to extract the specific flow features by building reduced-order models [45].

Other factors are involved in the thrombogenic process within LAA, such as cardiac condition, remodeling processes, and rheology [5]. Due to its complexity and multifactorial nature, this problem has been addressed by studying the individual effect of assuming (a) a rigid LA wall [30, 32], (b) blood as a Newtonian fluid [25], (c) different boundary conditions [46] or (d) different flow-split ratios [33, 47].

Many studies have used idealized geometries [48, 49] due to the difficulty in obtaining patient-specific geometries. This limitation has been overcome in recent years. However, idealized geometries are still used for experiments [46], to address particular processes [28, 49] or to test new methodologies to assess thrombus risk formation in LAA [50]. However, other medical data are required and difficult to obtain. The restrictions of medical data are (i) a limited number of patient-specific geometries, (ii) dynamic CT scans that cover the entire cardiac cycle are not commonly used during clinical practice, and (iii) PV and MV velocities synchronized with CT scans.

Advances in morphing techniques have helped to address the first restriction by modifying a particular geometry [36] or generating synthetic geometries [28, 50]. Regarding wall movement, the amount of radiation prevents physicians from taking multiple images during the cardiac cycle, and only a few studies have registered and interpolated endocardial images to obtain atrial movement [19, 30, 32]. This lack of atrial imaging can be compensated by introducing a kinematic model [51, 52, 24]. This model also offers the possibility of isolating the effect of AF from the particular anatomy, allowing a better comparison between different endocardial models [53]. Finally, many studies employ boundary conditions taken from the bibliography when measurements are not available [54, 27, 44, 41].

In addition, a Universal Left Atrial Appendage Coordinates (ULAAC) system has recently been introduced [45] to

allow visualization, analysis, and comparison of results from a wide variety of LAA morphologies.

Although almost all aspects related to LA seem to have been studied, little attention has been paid to the influence of PV on LA flow. From an anatomical point of view, around 70 % of the population has 4 PV [1, 7, 55], ranging the number of PV from 3 to 7 [6, 56, 55]. The dimensions of PV are important for clinical purposes [57, 58] because there is a lower risk of thrombus appearance when the PV section increases [28]. The location of the PV within LA also affects the LA flow and the velocity profile of the MV [59, 60, 47]. In fact, a comparison between the groups with/without a history of stroke has shown a difference in the angle between the orifices of the left/right PV and the LAA ostium in both groups [58]. Therefore, the orientation of the PV is a parameter to consider when assessing stroke risk.

The orientation of the PV is clinically a critical factor because it hinders catheter manipulation during the ablation procedure and affects AF recurrence after the procedure [61, 62, 63]. However, the number of CFD studies that include it as a parameter to assess stroke risk is reduced. Dueñas et al. [36] morphed an atrium to modify the orientations of its PV, obtaining geometries whose orientations were the mean and extreme physiological values previously reported in the bibliography. The results confirmed how variations in the orientation of the PV can affect stasis within the LAA. Recent studies [56, 17] with a large cohort of patients reported that the angle between left PV (LPV) and the angle between RPV influence the formation of flow structures within the LA. These studies also pointed out that the orientation of the RPV determines if the atrial flow is oriented directly to the MV, as also shown in [47]. All of these studies [56, 36, 17, 47] confirmed that the influence of the angles of PV on blood stasis should not be ignored under AF conditions, highlighting the need to better understand the relationship between PV orientations and blood stasis within the LAA.

Although large cohorts were studied [56, 17], their results combine several structural modifications (LAA and LA morphologies, PV locations and orientations), so the isolated effect of PV orientations was not analyzed. To our knowledge, only one study considers the isolated impact of varying the orientation of the PV [36]. However, they did not focus on understanding how the flow patterns were modified. A recent study has observed how different representative atrial flow patterns can be identified depending on the position of the main atrial vortex within the LA [47]. They observed how the main atrial vortex varies its position with the flow split ratio, suggesting that its position may also vary depending on the PV orientation.

To meet the above challenges, our study aims to perform an exhaustive analysis to highlight the influence of PV orientations on atrial flow patterns and, specifically, its effect on LAA stasis. We will illustrate how the position of the main atrial circulatory flow depends on the LPV orientations and flow split ratio. In addition, we will show how the main atrial circulatory flow interacts with the RPV flow, affecting

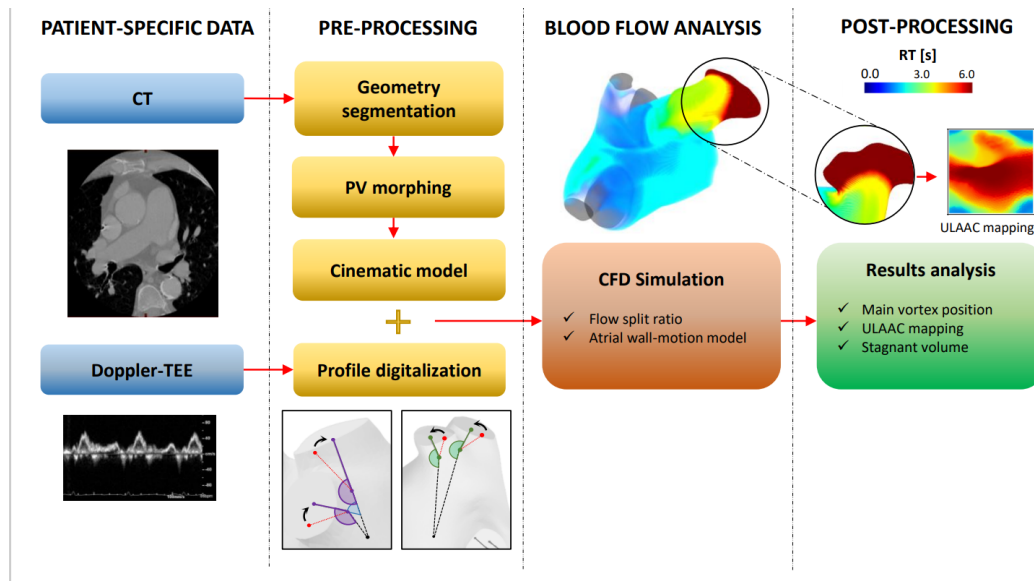


Figure 1: Workflow of the study. *Patient-specific data:* The initial data were CT images and Doppler TEE. *Data pre-processing:* CT images were segmented. The resulting atrial models were morphed to obtain several versions with different PV orientations. Boundary conditions were obtained for each case from a cinematic model, a CFD-ready volumetric mesh, and PV Doppler curves. *Flow analysis:* Two simulations with different flow split ratios were run for each case. *Post-processing:* The ULAAC system was used to project multiple indices and for results comparison.

the LAA washing. To the best of our knowledge, this has not been done in a parametric manner. To this end, we have selected two patients with the most different atrial flow patterns from the previous literature [47]. We have gradually modified their LPV and RPV orientations to transition from one flow pattern to the other and vice versa, demonstrating in a parametric manner how the PV orientation plays a fundamental role in the formation of the atrial flow patterns. Therefore, showing in which way the orientations of LPV and RPV affect LAA stasis and thus may influence the risk of thrombosis in the medium and long term.

2. Methods

As mentioned, this work aims to study the influence of the orientation of PV on LA flow, as it can strongly influence blood renewal within LAA. In a previous work [47], it was found that atrial geometries can be classified into two representative atrial flow patterns (types A and B) depending on the stasis response to changes in the flow-split ratio. This response was reported to depend on the position of the center of the main circulatory flow: When it is located right after the LPV, the atrial flow pattern is Type A, whereas if it is located near the LAA ostium or close to the LA roof, it is Type B. To demonstrate how the PV orientations define the formation of these atrial flow patterns, we modified the PV angles of a Type A atrium to obtain a Type B behavior (transition AB) and vice versa (transition BA). The complete framework involved CT scanning, geometry segmentation, anatomical morphing, Doppler TEE digitalization, wall motion implementation, CFD simulation, and post-processing. The current workflow is summarized in Figure 1.

2.1. Clinical data

As mentioned, two patients with different atrial flow patterns were selected from our database (Table 1). Both participants provided their informed written consent according to the guidelines of the Declaration of Helsinki. The Ethics Committee of the University Hospital of Badajoz (Spain) and the University of Extremadura authorized the study.

The velocity in each PV and mitral valve (MV) was measured using EPIC CVx and Affiniti CVx cardiovascular ultrasound systems (Philips, The Netherlands). An in-house code, written in Matlab® (Mathworks, Inc, Natick, MA, USA), digitalized these velocity profiles.

CT scans were obtained using a LightSpeed VCT General Electric Medical Systems scanner (Milwaukee, WI, USA). The Doppler waveforms were synchronized as the TEE and CT scans were acquired at different instants. PV measurements were used to impose boundary conditions for the inflow, while MV measurements were used to validate the simulation.

Each set of CT images was segmented following a semi-automatic procedure [30]. The segmentation process was supervised by two experts, a radiologist and an interventionist cardiologist. Two surface meshes were generated, one for each anatomy in 0%RR. RR is the time between two consecutive electrocardiographic R waves, i.e. patient-specific duration of the cardiac cycle, where 0%RR stands for electrocardiographic end-diastole of the ventricle. An open-source 3D software, Blender 3.2 [64], was used to clean and adjust the meshes for a subsequent simulation. Figure 2 shows the geometry resulting for each patient.

Table 1
Clinical data

	Age [years]	Sex [M/F]	Clinic history	Af type	LA volume [mL]	HR [bpm]	LAA volume [mL]
Patient 1 - Transition AB	89	F	HT/DLP	PE	114-138	50	10
Patient 2 - Transition BA	83	M	HT	PA	153-175	75	19

HT - hypertension; DLP - cholesterol; HR - heart rate; PE - Permanent; PA - Paroxysmal

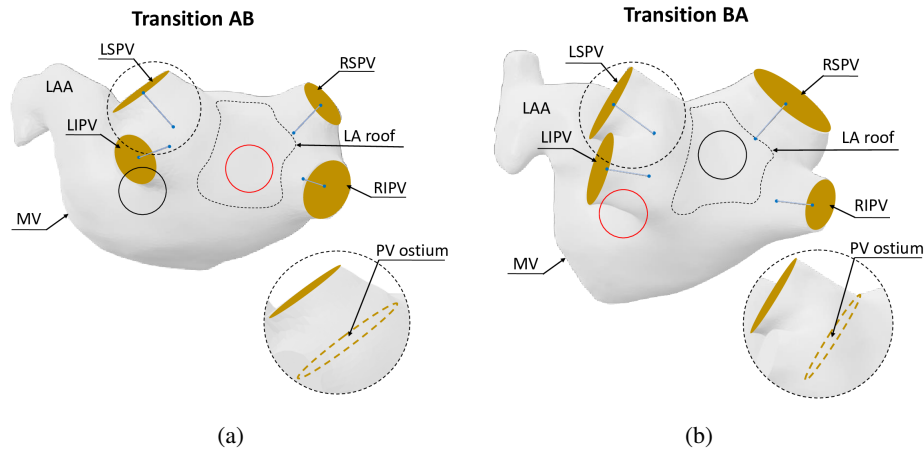


Figure 2: Patient-specific geometries for both patients. Regions enclosed by dashed lines represent LA roof areas. Black and red circles represent the initial and final position of the main circulatory flow, respectively, in both cases. A yellow dashed circle depicts the PV ostium area in the zoomed region.

2.2. Anatomical morphing

2.2.1. Geometrical parametrization

We used a methodology similar to that proposed by Mill *et al.* [17] to parameterize the orientations of the PV, but selecting the coronal and axial planes as a reference to define the characteristic angles (Figure 3). We adopted these anatomical planes as a reference because they are widely used in common clinical practice and will facilitate the comparison of different anatomies [36]. The angles were defined

as follows. Two segments were defined for each PV and reference plane, one segment from the center of the PV cut (yellow surface in Figure 2) to the center of the PV ostium (yellow dashed lines in Figure 2), and another segment from this point to the atrial center of gravity. Angles Φ_i and δ_i were defined between the PV segments in the coronal plane (Figure 3a) and the axial plane (Figure 3b), respectively. Angles α and β were defined in the coronal plane between LPV and RPV, respectively (Figure 3a). Lastly, Figure 3

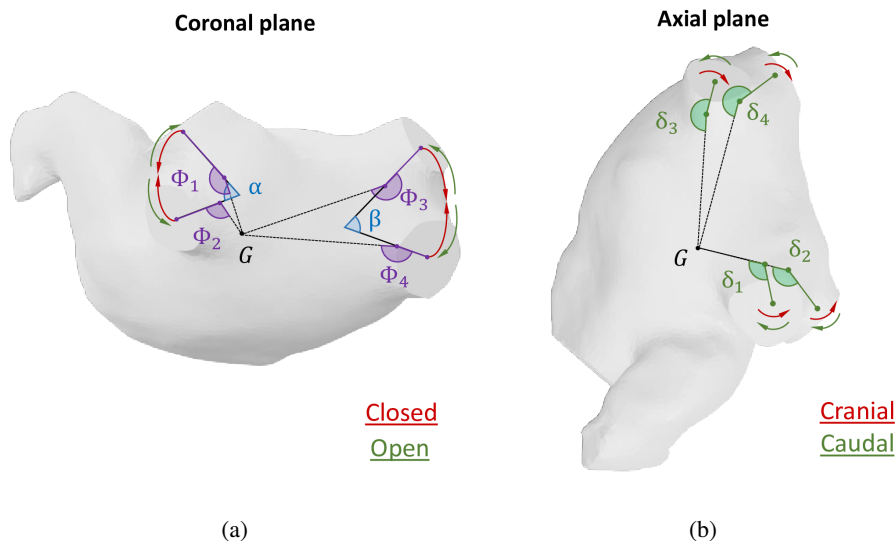


Figure 3: (a) Φ_i , α , and β angles defined in the coronal plane. (b) δ_i angle defined in the axial plane.

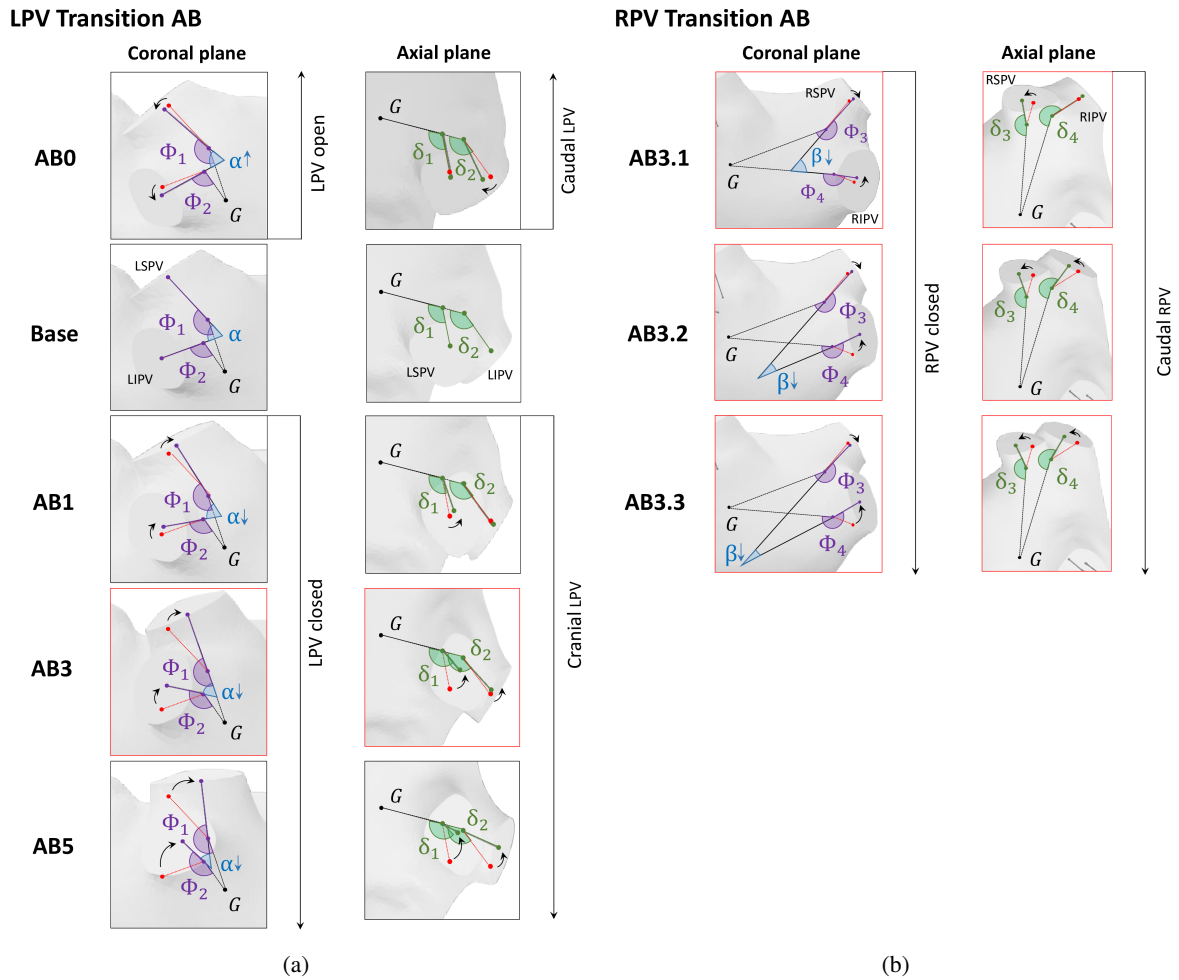


Figure 4: PV angle transformations in the coronal (purple) and axial plane (green) with respect to baseline case segments (in red) for Transition AB. (a) LPV transformations to change the position of the main atrial circulatory flow, and (b) RPV transformations to direct the RPV flow to the new position of the main atrial circulatory flow.

Table 2
Angular combinations applied for transitioning a type A case flow pattern into a type B.

Cases	Transition AB									
	Coronal plane						Axial plane			
	Φ_1	Φ_2	Φ_3	Φ_4	α	β	δ_1	δ_2	δ_3	δ_4
AB0	140	90	211	170	72	65	113	132	192	219
Base	155	105	211	170	70	65	118	140	192	219
AB1	167	118	211	170	66	65	123	148	192	219
AB2	175	124	211	170	66	65	132	150	192	219
AB3	177	132	211	170	62	65	140	152	192	219
AB4	183	144	211	170	57	65	148	158	192	219
AB5	191	167	211	170	43	65	160	169	192	219
AB3.1	177	132	207	175	62	54	140	152	167	218
AB3.2	177	132	205	207	62	21	140	152	160	197
AB3.3	177	132	205	214	62	14	140	152	155	189

also shows the standard clinical criteria for referring to the different PV orientations: open/closed (coronal plane) and cranial/caudal (axial plane).

2.2.2. LA rigging and skinning

The 3D segmented geometries were rigged and skinned following the method proposed by Dueñas *et al.* [36] to obtain different PV orientations. We used Blender 3.2, an

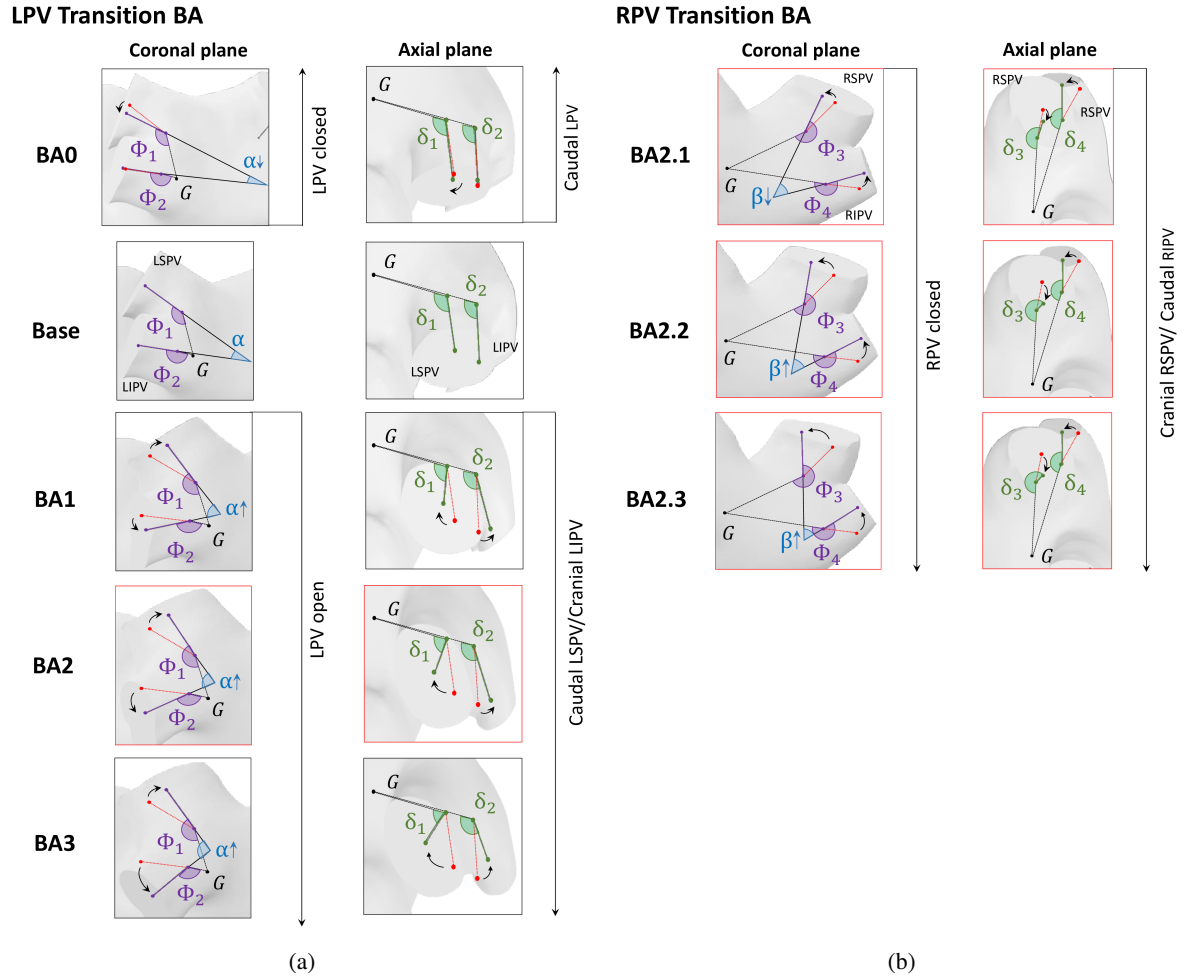


Figure 5: PV angle transformations in the coronal (purple) and axial plane (green) with respect to baseline case segments (in red) for Transition BA. (a) LPV transformations to change the position of the main atrial circulatory flow, and (b) RPV transformations to direct the RPV flow to the new position of the main atrial circulatory flow.

Table 3

Angular combinations applied for transitioning a type B case flow pattern into a type A.

Cases	Transition BA											
	Coronal plane						Axial plane					
	Φ_1	Φ_2	Φ_3	Φ_4	α	β	δ_1	δ_2	δ_3	δ_4		
BA0	131	168	198	179	16	54	120	99	175	139		
Base	144	166	198	179	27	54	108	101	175	191		
BA1	164	146	198	179	71	54	94	118	175	191		
BA2	173	129	198	179	95	54	81	128	175	191		
BA3	173	112	198	179	111	54	63	128	175	191		
BA2.1	173	129	219	208	95	48	81	128	205	163		
BA2.2	173	129	236	216	95	54	81	128	220	162		
BA2.3	173	129	246	225	95	59	81	128	285	158		

open-source 3D suite with full rigging and morphing capabilities [64]. First, the rigging process provided each atrial geometry with an armature formed by different bones. For each atrial geometry, the following bones were defined: right superior PV (RSPV), right inferior PV (RIPV), left superior PV (LSPV), and left inferior PV (LIPV). Each bone was defined between the center of the PV cut and the center of

the PV ostium, shown in Figure 2 as blue segments. Second, for the skinning process, the *envelope technique* was applied [64]. This technique uses the *heat algorithm* [65] to calculate the influence region for each bone based on its distance from the surrounding points. Each bone controlled the mesh vertices under its influence, allowing us to modify the PV orientations by selecting the characteristic angles Φ_i and δ_i .

2.2.3. LA morphing

We will now describe the morphing process that has allowed us to transform the atrial flow patterns by only modifying the characteristic angles of PV: *Transition AB*, from type A to type B, and *Transition BA*, from type B to type A.

Transition AB: To perform this transition, the following two conditions must be met: (i) the main circulatory flow should be displaced from near the exits of the LPVs (black circle in Figure 2a) to the region near the LA roof and the RPVs (red circle in Figure 2a), and (ii) the RPVs should be oriented toward this new position of the main circulatory flow. Once the transformation is complete, it should be checked that the RT increases in the modified geometry when the flow split changes from 59-41% to 37-63% LPV-RPV, as this is the main feature of type B anatomies [47].

Requirement (i) is gradually achieved by decreasing α and increasing Φ_1 and Φ_2 , as can be seen in Figure 4a (cases AB1-5). Decreasing α reduces interference between LPV flows and, with increasing Φ_1 and Φ_2 , allows the main circulatory flow to move toward the LA roof, far from the exits of the LPV.

Requirement (ii) is achieved by directing the RPV flow to the new position of the main circulatory flow, i.e., increasing Φ_4 and decreasing Φ_3 , β , δ_3 , and δ_4 . Modifications to the characteristic angles of RPV for the transition AB are shown in Figure 4b (cases AB3.1-3.3). Table 2 summarizes the characteristic angles of the morphed geometries generated during the AB transition.

Transition BA: To perform this transition, the following two conditions must be met: (i) the main circulatory flow should be displaced from the LA roof (black circle in Figure 2b) to the region near the exits of the LPV (red circle in Figure 2b), and (ii) the RPV flow should be oriented toward the MV. Once the transformation is complete, it should be checked that the RT decreases in the modified geometry when the flow split changes from 59-41% to 37-63% LPV-RPV, as this is the main feature of type A anatomies [47]. This is due to a slight displacement of the center of the circulatory flow toward the LAA ostium, which favors LAA blood renewal.

Requirement (i) is achieved by gradually decreasing Φ_2 and increasing Φ_1 and α , as can be seen in Figure 5a (cases BA1-3). Increasing α brings forward the collision between the LPV flows and, together with decreasing Φ_2 and increasing Φ_1 , allows the main circulatory flow to move towards the exits of the LPV, far from the LAA roof. Requirement (ii) is achieved by directing the RPV flow to the MV, increasing Φ_3 , Φ_4 , and δ_3 , and decreasing δ_4 . Modifications to the characteristic angles of the RPV for the BA transition are shown in Figure 5b (cases BA2.1-2.3). Table 3 summarizes the characteristic angles of the morphed geometries generated during the BA transition.

2.3. Parametrization of the LA wall motion

Applying the transitions to patient-specific geometries results in a set of morphed geometries (10 for the first patient and 8 for the second). These generated geometries lack

any information regarding the LA displacement field, so an atrial cinematic model was employed to recreate the atrial wall motion. This displacement was generated following the methodology described by Zingaro *et al.* [52], which was also employed in several recent works [24, 47, 51, 53]. Following this method, we calculated the atrial boundary velocities from patient-specific flow profiles obtained from Doppler velocities.

2.4. Patient-specific numerical model

Tetrahedral meshes were generated for each geometry 0% RR using the software ANSYS® MeshingTM (ANSYS, Inc.). A mesh convergence study was performed to verify that the mesh resolution did not significantly affect hemodynamics and stress results. The differences between the results of the selected mesh and a more refined one were less than 1%. The number of cells in the selected meshes ranged from 1.5M to 2M, depending on each case.

The simulations were performed using ANSYS® Fluent software (ANSYS, Inc.). The advection and transient schemes were second-order accurate and a 10^{-4} convergence criterion was established for the residuals. A coupled scheme was selected as the pressure-velocity coupling algorithm.

The wall motion generated by the kinematic model described in §2.3 was prescribed by applying the dynamic mesh capabilities of ANSYS®. The node diffusion algorithm was selected as part of the smoothing method, using cell volume as a diffusion function. As both patients suffered from AF, atrial motion was severely reduced and remeshing was not necessary.

As stated in §2.1, Doppler velocity measurements in the PV allowed imposing patient-specific boundary conditions at the inlets, while the measurements in the MV gave the possibility of validating the simulation results. An inlet flow and a constant outlet pressure were imposed as boundary conditions. The inlet flow was adjusted to generate the different flow split cases: 59-41% and 37-63% LPV-RPV.

Blood was considered a non-Newtonian fluid following Carreau's model [66]. The fluid density was assumed to be $\rho = 1050 \text{ kg/m}^3$ and the dynamic viscosity μ was obtained from the following expression:

$$\mu = \mu_\infty + \omega (\mu_0 - \mu_\infty) \left[1 + (\lambda \dot{\gamma})^2 \right]^{\frac{n-1}{2}}, \quad (1)$$

where $\dot{\gamma}$ is the shear rate, $\mu_\infty = 0.00345 \text{ Pa} \cdot \text{s}$ and $\mu_0 = 0.056 \text{ Pa} \cdot \text{s}$ are the infinite and zero shear rate viscosities, $\lambda = 3.31 \text{ s}$ is the characteristic time, and $n = 0.3568$ is the power law index. All these values have previously been measured [67]. ω is a dimensionless number to introduce the non-Newtonian character ($\omega = [0, 1]$ would shift from a Newtonian to a Carreau model).

Pressures and velocities were obtained by solving the continuity and Navier-Stokes equations (Eqs. 2 and 3, respectively):

$$\nabla \cdot \mathbf{v} = 0 \quad (2)$$

$$\frac{\partial \mathbf{v}}{\partial t} + \mathbf{v} \cdot \nabla \mathbf{v} = -\frac{\nabla p}{\rho} + \frac{\mu}{\rho} \nabla^2 \mathbf{v} \quad (3)$$

where \mathbf{v} is the velocity vector and p is the pressure.

A time convergence analysis was performed: the velocity was monitored at several points distributed in the fluid domain, showing that all simulations reached a quasi-periodic regime after four cycles. Therefore, the following analyses shown in §3 are based on the results after the fourth cycle. The selected time step was $\Delta t = 0.001$ s, as no variation was detected in the simulation results when it was halved.

2.5. Hemodynamic indices

We have calculated the moments of age [68] to delineate stagnant blood regions similarly to our previous work [30, 36, 45, 69]. The m_k age moment can be obtained as:

$$m_k = \int_0^\infty t^k f(t) dt, \quad (4)$$

where $f(t)$ is the age distribution of the blood and t is the simulation time. Fluent User-Defined Functions were used to integrate the moment equations of the age distribution into the solver.

The first moment of the age distribution m_1 is the blood residence time (RT). The normalized first moment M_1 can be obtained as:

$$M_1 = \frac{m_1}{\sigma}, \quad (5)$$

where σ is the standard deviation of m_1 and can be obtained as:

$$\sigma = \sqrt{m_2 - m_1^2}. \quad (6)$$

M_1 follows a bimodal distribution within the LAA [30], which allows automatic delimitation of the stagnant volume by selecting a patient-specific threshold. The selected threshold was the minimum probability valley between the two modes.

Some wall shear-based indices were also used for this study, such as the time-averaged wall shear stress (TAWSS) and the oscillatory shear index (OSI). Their formal definition is as follows:

$$\text{TAWSS} = \frac{1}{T} \int_0^T |\text{WSS}| dt. \quad (7)$$

$$\text{OSI} = \frac{1}{2} \left(1 - \frac{|\int_0^T \text{WSS} dt|}{\int_0^T |\text{WSS}| dt} \right). \quad (8)$$

TAWSS is commonly used as a thrombosis indicator, since low values are associated with endothelial cell damage [70]. OSI is a non-dimensional index that captures oscillations in the wall-shear direction, ranging between 0 and 0.5.

2.6. Universal left atrial appendage coordinates

The universal left atrial appendage coordinate (ULAAC) system [45, 47] was used to facilitate the visualization and comparison of data from different models. The method was inspired by the universal atrial coordinate (UAC) system of Roney et al. [71], which in turn evolved from the universal ventricular coordinates (UVC) by Bayer et al. [72]. To this end, the LAA surface of both patients was mapped to the unit square by solving two Laplace–Beltrami equations and using some anatomical landmarks as boundary conditions. The Laplace–Beltrami equations were solved using Python LaPy [73, 74].

3. Results

Thirty-six atrial simulations were performed since two different flow split ratios (59-41 and 37-63 % LVP-RPV) were considered for each of the 18 generated cases. All simulations were performed considering a prescribed wall motion and a non-Newtonian model. The cases are distributed as follows:

- 10 of these cases correspond to transition AB (Figure 4), summarized in Table 2.
- 8 of these cases correspond to transition BA (Figure 5), summarized in Table 3.

3.1. Representative atrial flow patterns

Our main objective was to deepen the understanding of the relationship between PV orientations and LA flow patterns. This phenomenon is important because it affects LAA washing and the risk of medium- and long-term thrombosis. To this end, and as mentioned in §2, we have modified the PV angles to gradually obtain transitions from the type A to type B atrial flow pattern and vice versa [47]. In an effort to isolate the influence of the PV orientations, we have kept the rest of the parameters constant for each anatomy: cardiac output, atrial motion, LAA volume, morphology, etc.

The first step was to identify the atrial flow patterns for both transitions, which was achieved by analyzing the blood streamlines. Figure 6 represents the blood streamlines when the flow structures are fully developed in 90%RR.

Regarding Transition AB, as stated previously, the LPV angles were modified so that the LPV were progressively closed. During the modification of the LPV, the center of the main circulatory flow moved from the LPV towards the LA roof. This can be seen in the streamlines for the cases AB1-AB5 in Figure 6a, where the flow-split ratio 59-41% was displayed to improve visualization of the main circulatory flow. These cases present a negligible interaction between LPV and RPV flows (colored LPV streamlines did not interact with gray RPV streamlines, Figure 6a), making it necessary to modify the RPV orientations to complete the AB transformation.

Case AB3 was selected as the starting point for the RPV transformation, as it presented more streamlines entering the LAA and, thus, better washing. As described above, the

RPV transformation implies providing the RPV a caudal orientation in the axial plane while closing them in the coronal plane. An increasing interaction can be seen in the streamlines in Figure 6b between the RPV and LPV flows for cases AB3.1-3.3. Simulations with a flow-split ratio of 37-63% are shown for these cases, since this LPV-RPV flow interaction does not occur for 59-41%. The transformation from a type A to a type B atrial flow pattern is now complete.

As stated above, the LPV were opened in the coronal plane in the transition BA. Figure 6c shows how, for cases BA1-3, the main circulatory flow changes its rotation direction and progressively moves toward the exit of the LPV. Similarly to Transition AB, 59-41% cases are shown to improve visualization of the main circulatory flow. The streamlines show how the washing of the LAA gradually becomes more governed by the LPV flow. However, pointing the RPV flow directly towards the MV is still necessary to complete the transformation to type A.

Case BA2 was selected as the starting point for the RPV transformation, as it presented a well-defined circulatory flow at the exit of the LPV: the center of the circulatory flow is clearly visible, and the RPV flow just surrounds it. After surrounding the center of circulatory flow, the RPV streamlines enter LAA (see case BA2 in Figure 6d where only gray streamlines can be observed in LAA). For BA2.1-2.3 cases, the superior RPV were gradually oriented cranially, while the inferior RPV were oriented caudally. Figure 6d also shows how RPV flow drives the main circulatory vortex near the ostium, improving LAA washing. Case BA2.3 shows how LPV flow is responsible for LAA washout in 37-63% (only color streamlines can be observed in LAA). This reproduces the typical behavior of a type A atrial flow pattern, so the BA transformation is complete.

3.2. Analysis of the vortex structures

The results of the previous section can be confirmed by analyzing the atrial vortex structures. Figure 7 shows the vortex structures of the AB and BA transitions at different instants of the cardiac cycle. The chosen instants correspond to diastole, as during systole, when the MV is closed, it is impossible to detect a main vortex structure. The first instant corresponds to the maximum blood flow through the PVs (64.5%RR). The second corresponds to the instant when the maximum vortex structure development is achieved (81.3%RR). Finally, the third corresponds to the instant of the MV closure (100%RR).

Figure 7a shows the comparison of the vortex structures between the initial (Base case - Type A flow) and the final morphology (Case AB3.3 - Type B flow) for the AB transition. The vortex structures are not visible for both cases in 64.5% RR, as the flow patterns are not fully developed. The maximum vorticity values are reached near the PV. The main vortex structures are fully developed at 83.3%RR, varying their location from LPV (Base case) to LA roof (Case AB3.3). Moreover, the vorticity value is reduced from 64.1 s^{-1} to 32.3 s^{-1} . Finally, at MV closure, the vortex morphology of the Base case is almost conserved, while it

is substantially modified for Case AB3.3, where the vortex structures with lower vorticity values are dissipated.

Regarding the BA transition, Figure 7b also compares the vortex structures between the initial (Base case - Type B flow) and the final morphology (Case BA2.3 - Type A flow). Following the same criterion as in the AB transition, three instants were selected when MV was opened. The high inflow at 65.5%RR marks the beginning of the formation of vortex structures. As in transition AB, vorticity values peak at this instant. The vorticity values are significantly higher for transition BA ($\sim 200 \text{ s}^{-1}$). The complete development of the main vortex structures occurs at 81.3%RR. At this stage, the vortex structures are concentrated near the LPV (case BA2.3), following the behavior of a type A atrium (Base case in Figure 7a). In contrast, the base case shows a hectic flow structure close to the LA roof, following the behavior of a type B atrium. This structure is further fractured when the MV is closed, similar to Case AB3.3 (Figure 7a). On the other hand, Case BA2.3 concentrates its vortex structures around LPV, its vorticity value being similar to the base case in Figure 7a.

Finally, Figure 7c shows the influence of the flow split ratio when the main vortex structures are fully developed (83.3% and 81.3%RR for transitions AB and BA, respectively). For transition AB, the vortex structures are disordered by the collision of the RPV flow with the main vortex of the LPV when the flow split ratio is changed to 37-63%LPV-RPV. Regarding the BA transition, the main vortex is pushed towards the LAA ostium by the RPV flow when the flow split ratio is changed to 37-63%LPV-RPV.

3.3. Left atrial appendage residence time

Streamlines and vortex structures have shown that LA flow patterns can be substantially modified when changing the PV orientation. As LA flow patterns govern LAA washing, these changes in the PV orientation should lead to alterations in the RT within the LAA. Figure 8 shows RT/RT_{\max} contour evolution for all PV orientations (columns) for the flow splits under consideration. For each patient, RT is normalized with its maximum value, RT_{\max} . Figure 8a depicts RT/RT_{\max} evolution for the transition AB. When the LPV orientation is modified (AB0-AB5) while keeping the flow split at 59-41%LPV-RPV (see §2.2), RT/RT_{\max} gradually decreases until it reaches a minimum in Case AB3, growing afterward. RT/RT_{\max} increases in cases AB4 and AB5 because Φ_1 exceeds 180° and the original flow direction is reversed. A similar trend is observed when the flow split ratio is changed to 37-63%, but RT/RT_{\max} decreases with respect to 59-41%. Therefore, as described in §3.1, the modification of the RPV orientation is necessary to complete the transition AB (see the cases AB3.1, AB3.2 and AB3.3 in Figure 8a).

Figure 8b shows the evolution of the contour RT/RT_{\max} for the BA transition. In this transition, the values of RT/RT_{\max} increase when the LPV orientations are modified (BA0-BA3). This increase is more noticeable for the 37-63% flow split. As explained above, a change in the RPV orientation is

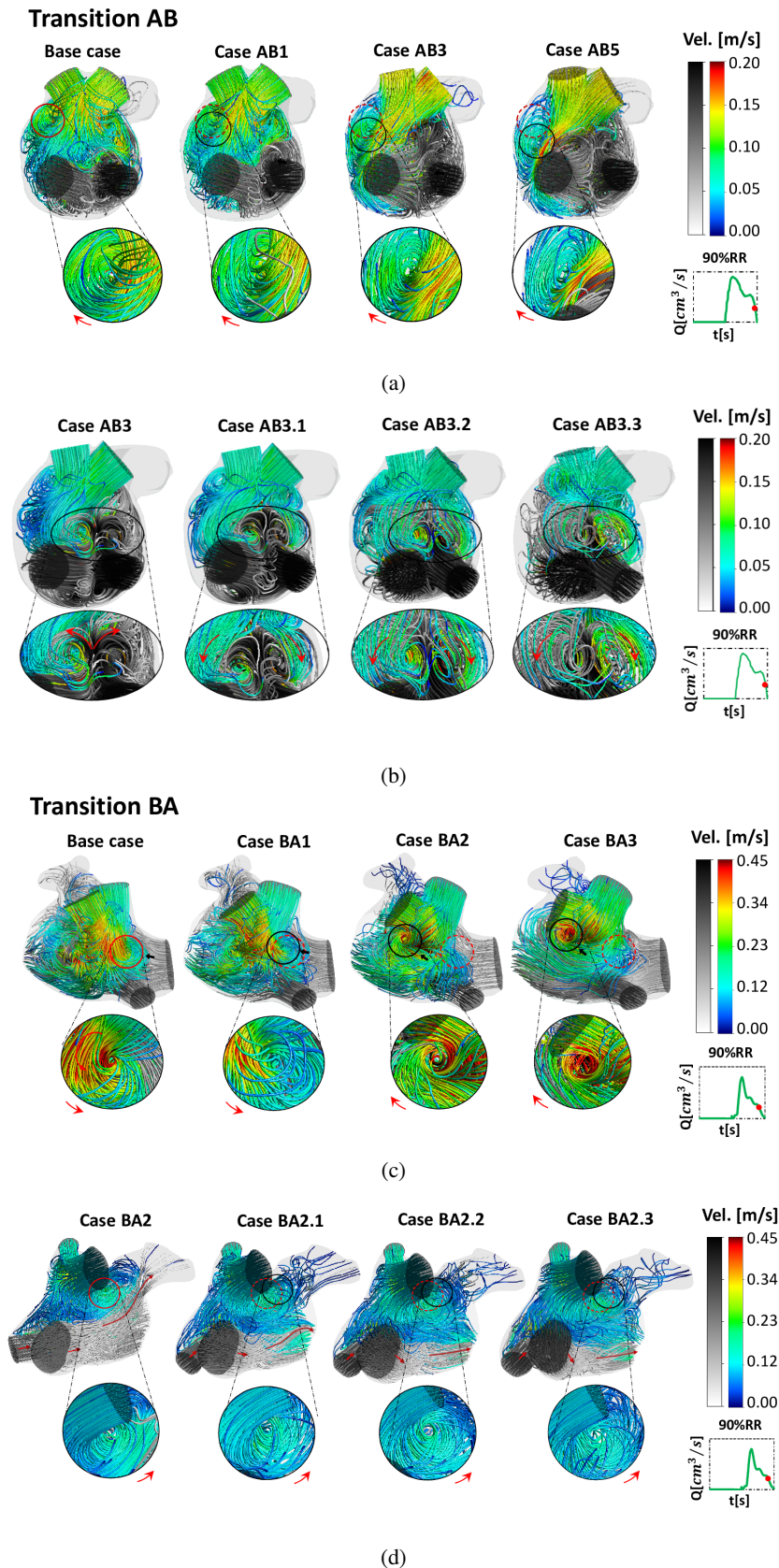


Figure 6: Blood flow streamlines at 90%RR for transitions AB (a,b) and BA (c,d). The color (gray) scale represents the velocity magnitude of the flow entering LA through the LPV (RPV). Red circles represent the position of the center of the circulatory flow in the base case. In contrast, the black ones represent the position when the PV orientation is modified. Subfigures (a,c) and (b,d) correspond to a 59-41% and 37-63% LPV-RPV flow split ratio, respectively. LA has been rotated to facilitate flow visualization, and zooms were added. Arrows indicate the direction of rotation.

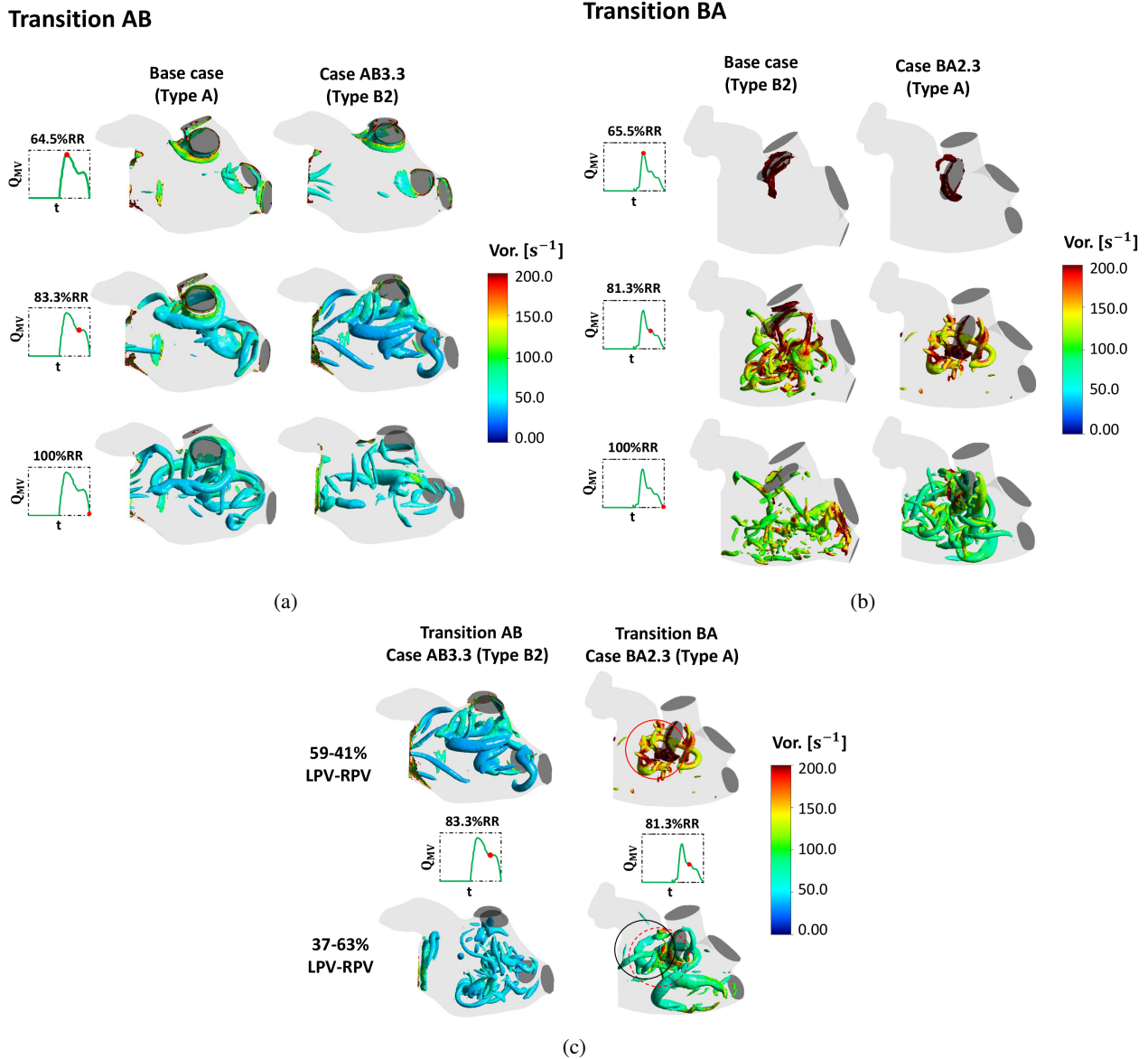


Figure 7: Vortex flow structures during systole for transitions AB (a) and BA (b), respectively. (c) Evolution of the main vortex structure when the flow split ratio changes from 59-41%LPV-RPV to 37-63%LPV-RPV. Flow structures were generated according to the q_2 criterion ($q_2 = 0.2$) and colored according to their vorticity value. The red circles indicate the initial position of the vortex, while the black circle marks the final position.

required to reverse this increase and complete the transition BA (see cases BA2.1, BA2.2, and BA3.3 in Figure 8b).

3.4. Stagnant blood volume evolution

An interesting parameter to delineate the stagnant region and thus determine the risk of stasis in the LAA is the stagnant volume. It was calculated as described in §2.5, and its evolution is depicted in Figure 9. Figures 9a and 9b graph the stagnant volume trend for the AB and BA transitions, respectively. The stagnant volume follows a trend similar to RT/RT_{max} . For the transition AB, it decreases when LPV are closed in the coronal plane (cranial orientation in the axial plane), reaches a minimum in case AB3, and increases slightly for cases AB4-AB5. Then, as mentioned, the RPV

are modified (caudal orientation in the axial plane) in the AB3.1-AB3.3 cases to achieve type B flow. This is reflected in Figure 9a, where the stagnant volume grows abruptly.

Regarding the BA transition, the LPV are opened in the coronal plane (the LSPV are caudally oriented and the LIPV are cranially oriented in the axial plane). Figure 9b depicts the evolution of the stagnant volume: In this transition, the minimal stagnant volume is found for the base case, as any modification in the LPV orientation leads to an increase. The highest value is reached for case BA3. When the RPV are modified (the RSPV cranially oriented and the RIPV caudally oriented), the stagnant volume drastically increases in case BA2.1 for the flow split ratio 59-41%LPV-RPV, slightly decreasing for 37-63%. The transition to type A is

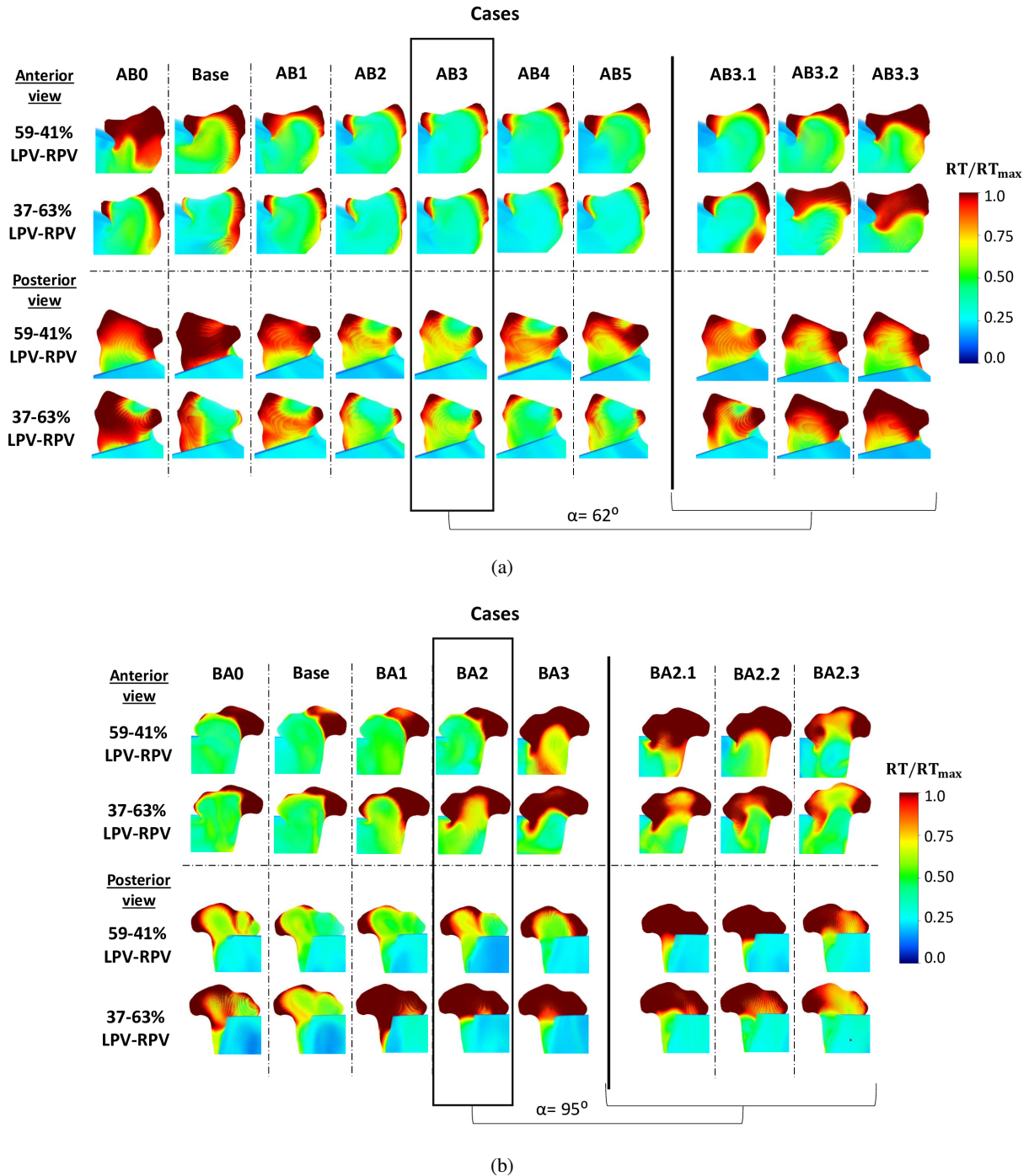


Figure 8: Stagnant volume for the different flow split ratios (rows), and PV configurations (columns) for (a) transition AB, and (b) transition BA. The cases are grouped according to the PVs that were modified (LPVs on the left and RPVs on the right).

confirmed when RPVs are further modified in the BA2.2-BA2.3 cases, as the stagnant volume decreases for the 59-41%LPV-RPV flow split ratio (it increases slightly and then decreases for the 37-63% LPV-RPV flow split ratio).

3.5. Hemodynamic maps

Figure 10 shows the hemodynamic maps for RT/RT_{max} , TAWSS and OSI, where RT was normalized using the

duration of the cardiac cycle. The hemodynamic indices were projected into the ULAAC system [45, 47] to facilitate the visualization and comparison of the data between the different cases. The layouts of the subfigures 10a and 10b are analogous: Each column represents a different PV orientation, while the rows correspond to the flow split ratio under consideration.

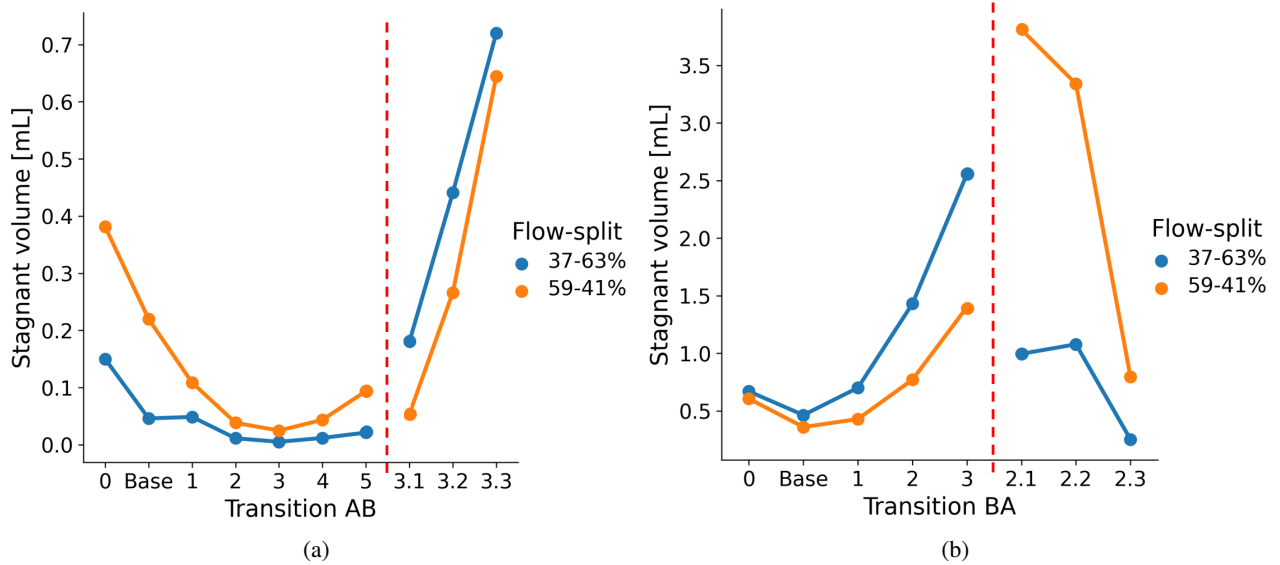


Figure 9: Evolution of the stagnant volume for the simulated cases for the transitions AB (a) and BA (b). The dashed vertical line separates the cases in which the LPV or the RPV are modified, respectively. Orange and blue lines represent the different flow split ratios under consideration.

RT/RT_{max} values in Figure 10a, validate the trend observed in sections §3.3 and §3.4 for the AB transition. All values progressively decrease, reaching a minimum in case AB3. The highest RT/RT_{max} values are concentrated in a narrow band located at the tip of the LAA. It should be mentioned that the RT/RT_{max} values are higher for the 59-41%LPV-RPV flow split, following the type A atrial behavior. This tendency is reversed by modifying the RPV orientation (shown in Cases AB3.1-3.3) and completing the AB transition.

TAWSS maps show the opposite trend compared to the RT/RT_{max} maps, showing low TAWSS values where the RT/RT_{max} showed high values. The lowest TAWSS values can be found in a narrow band near the LAA tip, whereas the highest values are located close to the ostium. Finally, OSI presents low values for all cases, indicating minimal flow oscillations barely affected by modifications in the PV orientations.

Regarding the BA transition (Figure 10b), there is a progressive increase in RT/RT_{max} values in the BA1-BA3 cases. These cases show the characteristic trend of type B, as evidenced by the higher RT/RT_{max} values observed for the flow split ratio 37-63%LPV-RPV. In contrast, the BA2.1-BA2.3 cases show a reverse flow split trend, indicating a complete transformation to type A. Between these BA2.1-BA2.3 cases, the lowest RT/RT_{max} value is shown in the BA2.3 case. It should be noted that after the transition BA the patient presents higher RT/RT_{max} values than in the base case. As for the previous transition, the TAWSS values show the opposite trend compared to RT/RT_{max} . The lowest values of TAWSS are found in a narrow band that corresponds to the LAA tip. Minimum values are reached in the flow split ratio 59-41% LPV-RPV for cases BA2.1-BA2.3. Lastly, the oscillations in the flow direction are more

affected by changes in the PV orientation and flow split ratio than in the previous transition. The lowest OSI values are shown in the base case (where the lowest RT/RT_{max} values and the highest TAWSS values are found), while the highest OSI values are concentrated in a region close to the tip of the LAA for the BA1-BA3 cases with a flow split ratio of 37-63%LPV-RPV, and for the BA2.1-BA2.3 cases with a flow split ratio of 59-41%LPV-RPV.

4. Discussion

Recent advances in computational modeling and medical imaging techniques and the growth in processing power make it possible to simulate patient-specific high-fidelity models, empower interdisciplinary collaborations, and drive a revolution in cardiovascular research. These synergies enable the generation of increasingly realistic digital twins to investigate pathological mechanisms, support the design and implantation of medical devices, and improve cardiac diagnosis.

With respect to AF, CFD techniques have allowed in recent years to deepen our understanding of the hemodynamic substrate in patients with AF ([45, 24, 32]). Together with patient-specific atrial segmentations, flow boundary conditions in the PV/MV, and wall motion reconstruction, these simulations provide an accurate 3D time-resolved representation of atrial flow. This time-resolved flow field allows calculation of hemodynamic indices related to blood stasis [36, 25, 41], such as residence time (RT) or wall shear-derived indices (TAWSS, OSI, etc.). The analysis of these indices is especially relevant within the LAA, where thrombi are more prone to form.

Most of the previous atrial CFD studies focused on the relationship between blood stasis and LAA morphology [28,

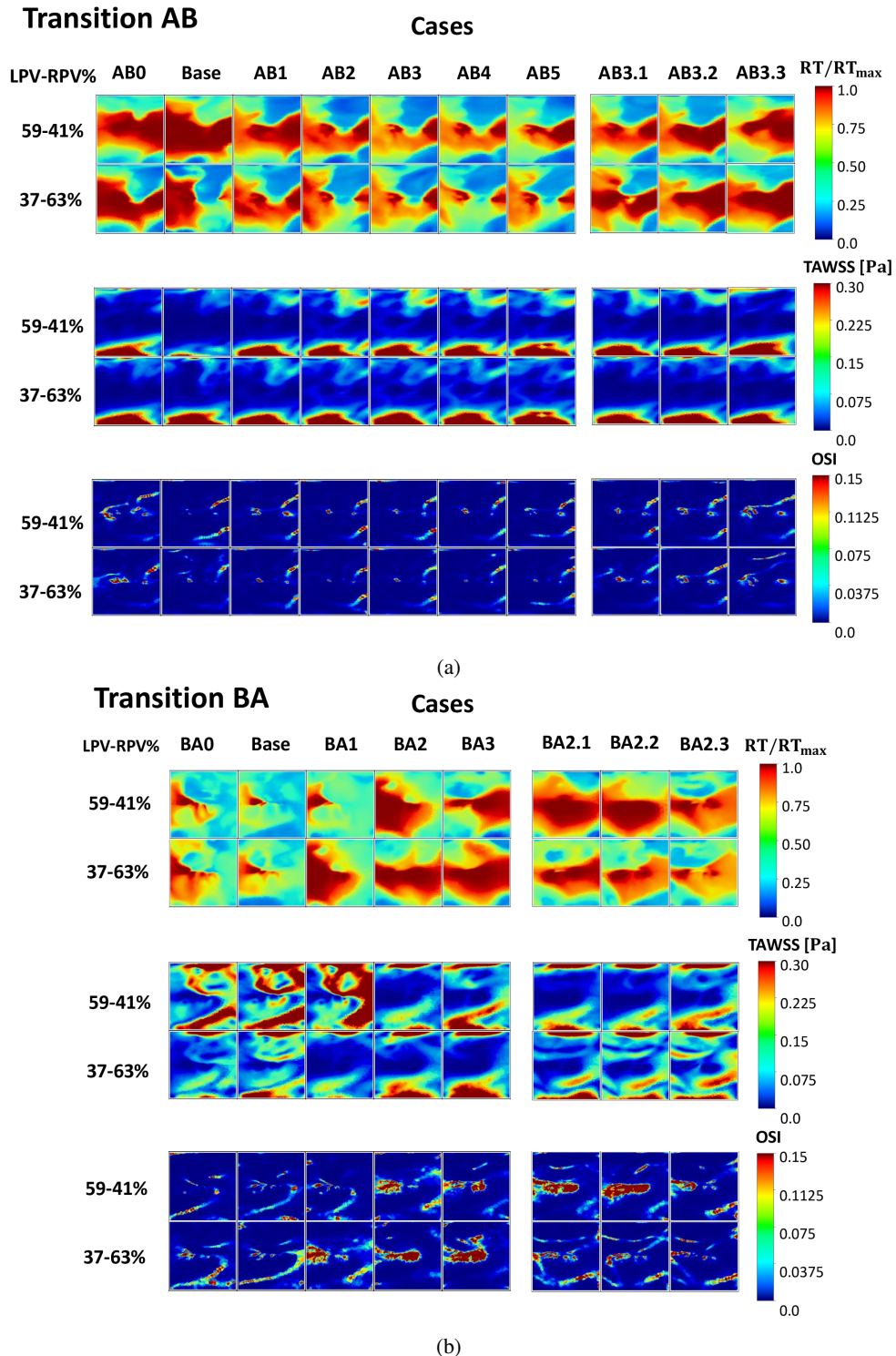


Figure 10: ULAAC projections of RT/RT_{\max} , TAWSS, and OSI for the transitions AB, (a) and BA (b). The columns show the evolution of the contours through the different PV configurations, while the rows show the changes due to the different flow split ratios considered.

29, 32], on contrasting different atrial modeling hypotheses [30, 33, 25, 44, 75], or on looking for the most suitable metrics to quantify stasis [30, 24, 37]. However, the translation of computational advances to improve clinical decisions about AF still faces significant challenges. For example, the

formation of a stagnant region within the LAA is highly dependent on atrial flow patterns and, particularly, on the position of the main atrial vortex in relation to the LAA [47]. However, atrial flow patterns depend on several parameters: LA/LAA morphology, PV orientations, cardiac output, flow

split ratio, wall motion, etc. Therefore, understanding the influence of each of these parameters will require isolating and studying its influence one by one instead of performing patient-specific simulations in which several parameters are simultaneously modified. Furthermore, the variation of these parameters depends on time: atrial remodeling can alter the LA/LAA morphology over months/years [5], while atrial wall motion and cardiac output can vary significantly throughout the day due to changes in cardiac conditions [76, 77, 78] (rest/exercise, sinus/fibrillated rhythm). Even the flow split ratio is highly dependent on the position of the patient [33, 79]. For these reasons, although these studies have contributed to a better understanding of AF phenomena and the boundary conditions that best reproduce atrial flow, they have not yet gone far enough to build a predictive understanding of each of their anatomical and functional determinants.

To meet the challenges described above, this manuscript will focus on achieving a better understanding of the influence of the PV orientations on the formation of the main atrial vortex and its implications on stasis within the LAA. Although it is confirmed that PV orientations affect stasis within the LAA [36, 56, 17], the number of CFD studies that include it as a parameter to assess stroke risk is reduced. Mill *et al.* [56, 17] studied several geometries, reporting the importance of the PV angles on atrial flow patterns. However, their simulation results combined several patient-specific modifications (LAA and LA morphologies, PV orientations), so it was impossible to analyze the isolated effect of PV orientations. Dueñas-Pamplona *et al.* [36] made a preliminary parametric approximation on a patient-specific basis to study the influence of PV on stagnant LAA volume. However, they only considered extreme PV configurations to quantify the maximum variation of stagnant volume without performing a gradual and exhaustive PV variation to understand its effect on different flow patterns. In fact, neither the formation of the main circulatory flow nor the various influences of varying LPV and RPV were studied.

To fill this gap, this work combined some recent methodological advances to better understand the relationship between PV orientations and the formation of the main atrial vortex, together with its implications for LAA stasis. The results highlight how the position of the center of this main atrial vortex is considerably altered by changes in the PV orientations and also, although to a lesser extent, by changes in the flow split ratio.

As is well known, the LPV flow is characterized by the formation of the main atrial vortex, while the RPV flow is mostly conducted directly towards the MV [21]. Our departure point was LA segmentations from two patients with AF (Figure 2, Table 1). Although we know this is a limited number of patients, the sample contained two extreme representative atrial flow patterns that can be identified depending on the position of the main atrial vortex [47]. Patient 1 presents a type A flow behavior, with the main atrial vortex forming just after entering the LA and near the LPV, while Patient 2 presents a type B flow behavior, with

the main atrial vortex being pushed toward the LA roof and near the RPV. It should be noted that this flow classification also implies different responses to changes in the flow split ratio: type A atriums will present a better LAA washing for a flow split ratio of 37-63%, while type B atriums will present a better LAA washing for a flow split ratio of 59-41%.

Second, a morphing methodology [36, 45] was applied to perform a geometric data augmentation. Specifically, the PV were rigged and skinned following the method proposed by Dueñas-Pamplona *et al.* [36] to obtain different PV orientations. To demonstrate in a parametric manner how the PV orientations play a fundamental role in the formation of the atrial flow patterns, the LPV and RPV orientations were gradually modified to transition Patient 1 from Type A to Type B (transition AB) and Patient 2 from Type B to Type A (transition BA). Completing these transitions highlights how the different flow patterns governing LAA washout are highly affected by PV orientation, as well as allowing separate studies of LPV and RPV. To achieve these transitions, two transformations should be performed: (i) the main atrial vortex should be displaced toward its new position by changing the LPVs orientation, and (ii) the RPVs should be oriented toward the main circulatory flow (transition AB) or towards the MV (transition BA). A methodology similar to that proposed by Mill *et al.* [17] was used to parameterize these transformations and measure the PV characteristic angles. In this work, we selected coronal and axial planes as a reference to define the characteristic angles, shown in Figure 3. This choice allowed us to generalize the proposed PV parameterization, as these planes are widely used in clinical practice and will facilitate comparison between different anatomies. The complete methodology is explained in detail in §2.2, and the PV transformations are detailed in Figures 4 and 5, and Tables 2 and 3. To isolate the influence of PV orientations, the rest of the parameters were kept constant during these transformations: cardiac output, atrial motion, LAA morphology, etc.

Depending on the patient-specific distribution of fibrosis, the motion of the atrial wall is altered during episodes of AF. To prevent this effect from introducing bias into our analysis and to homogenize the effect of fibrosis between patients, we used the same kinematic model as Rodríguez-Aparicio *et al.* [47], which was first proposed by [24, 52, 51]. This model allows to generate a smooth wall motion according to the patient-specific transmitral flow profile. Although this model may not capture all patient-specific flow characteristics, its efficacy in replicating LA and LAA hemodynamics is demonstrated [53], facilitating the isolation of geometrical and functional parameters and thus the study of PV orientations.

Regarding the rheology of the blood, we considered constitutive relations based on the Carreau model, which was widely used in previous CFD studies of cardiovascular flows [25, 80, 81]. Although Newtonian fluid assumption is widely used for cardiac cavities, as non-Newtonian atrial effects are reduced [28, 82], recently Gonzalo *et al.* [25] suggested that Newtonian effects can affect hemodynamics within the

LAA. These effects would shape the filling and draining jets, affecting the secondary swirling motions that govern LAA washing when LA wall motion is impaired.

The gradual flow transitions AB and BA were monitored by analyzing the transformations achieved in the blood streamlines, shown in Figure 6 for 90%RR, when the atrial flow structures are fully developed. Although it was already known that the LPV flow governs the main atrial vortex [83, 47], to the best of our knowledge, this is the first time that it has been demonstrated how the position of its center can be modified by changing the orientations of the LPVs. Moreover, the influence of RPVs is minor but not negligible. Their orientation determines the nature of their interaction with the main atrial vortex: they can either surround it and flow directly towards the MV or collide against it, generating a much more chaotic flow pattern. This chaotic flow pattern was previously observed [47], but the magnitude of this interaction was not previously studied by isolating the effect of gradually varying the PV orientations.

The transformation of the flow patterns was then confirmed by analyzing the vortex structures, whose evolution for both transitions is shown in Figure 7. We calculated the criterion q_2 , showing the vortex structures for $q_2 = 0.2$. This criterion is widely used to visualize vortex structures and assess flow characteristics [84, 85]. It was also used before for atrial flow [18, 19, 47]. Some representative time instants were selected to show the temporal evolution of the atrial flow structures for both transitions. The result confirmed that the maximum vorticity values are reached near the PV [19]. The main vortex structures are fully developed around 80%RR, and their location depends on the type of atrial flow. It can also be observed how the collision of the RPV flow with the main flow structure leads to a disordered and chaotic vortical structure throughout the atrial domain. These observations ratify previously observed flow patterns [47], confirming at the same time that the transitions AB and BA were completed.

Finally, the effect of variations in the PV orientations on LAA washing was assessed by means of hemodynamic indices. The gradual AB and BA transitions produced important changes in LAA stasis. Figure 8 shows clear patterns for RT/RT_{max} . The region with higher RT/RT_{max} values in the AB transition (Figure 8a) is affected by the position of the main atrial vortex (cases AB0-AB5), showing a minimum for the AB3 case. Regarding the influence of the flow split ratio, is noticeable but less important than that of the vortex position. The RT pattern is still type A, so RT is reduced when changing the flow split ratio from 59-41% to 37-63%. On the other hand, once RPV orientation is modified, the RT/RT_{max} values are affected by the magnitude of the interaction between the RPV flow and the main atrial vortex (cases AB3.1-AB3.3). It can be seen that as the RPV flow is gradually oriented towards the position of the main atrial vortex, this flow interaction worsens the LAA washing and increases RT/RT_{max} . When the AB transition is complete, the LAA washing is governed by RPV flow for a flow split ratio of 59-41%, becoming more chaotic and worsening the

LAA washing for 37-63%. An analogous RT pattern can be seen for the BA transition (Figure 8a). The RT/RT_{max} is affected by the position of the main atrial vortex (cases BA0-BA3), showing a minimum for the base case. The transition BA is completed when the RPV are oriented to the MV, allowing the development of the main circulatory flow towards the ostium and improving the LAA washing when changing the flow split ratio from 59-41% to 37-63%.

In addition to this analysis, the stagnant blood volume was calculated for each different case (Figure 9), showing a clear pattern for both transformations, analogous to the one commented before for RT/RT_{max} . Both transitions present smooth variations in the stagnant volume when varying the position of the main atrial vortex, with significant changes when the RPV orientation is modified and the transitions are completed. For better visualization and comparison, the wall results of RT/RT_{max} , TAWSS, and OSI were projected onto the ULAAC system (Figure 10). The patterns displayed for RT/RR and TAWSS are complementary, which is in agreement with the previous bibliography: Higher values of RT/RR are concentrated in a narrow band near the LAA tip, which coincides with lower values of TAWSS [45, 47]. Changes in the direction of flow within the LAA are more notable for the BA transition, although the OSI remains at low values. The cases with higher RT/RT_{max} have higher OSI values concentrated near the tip of the LAA, which is consistent with previous work [86]. This effect may be due to the combination of larger curvatures and low RT values present in this region.

Our work confirmed that the proximity of the main atrial vortex to the ostium can induce secondary swirling flows within the LAA that facilitate washing and prevent blood stagnation, which is consistent with previous work [33, 25]. However, the position of the main atrial vortex can be significantly modified by changes in the PV orientations and, to a lesser extent, by the flow-split ratio. We also confirmed that different types of atrial flow patterns have different LAA washing behaviors and responses to changes in the flow split ratio [47]. For the first time, we identified the relationship between the main atrial vortex and its interaction with the RPV flow, showing how this can be altered by changing the PV orientations, which, to the best of our knowledge, has not been done before. Moreover, we demonstrated how the atrial flow pattern and its response to changes in the flow split ratio can be totally reverted by an appropriate combination of transformations in the RPV and LPV orientations.

4.1. Clinical applications

In recent years, CFD techniques have shown their value in shedding light on multiple cardiovascular diseases, and even helping during cardiac diagnosis [87, 88]. Regarding AF, CFD contributed to quantifying stasis within LAA in a patient-specific basis and achieving a better understanding of atrial flow patterns and the prothrombotic substrate of the disease [28, 32, 30, 24]. This may facilitate the development of new tools to improve both diagnosis and treatment. However, while CFD studies have improved our understanding

of AF mechanisms, atrial flow, and the determination of otherwise inaccessible stasis-related parameters, the connection between atrial flow patterns and stasis in LAA remains unclear. This study aimed to investigate atrial flow patterns and their relationship to LAA washing, and more specifically how these were affected by variations in the PV orientations.

The findings of this study could have direct implications for the diagnosis of AF, as PV orientations are not taken into account during standard clinical practice when assessing the risk of stroke in a particular patient. We suggest introducing PV orientations in the characterization of the patient-specific risk of stroke, as it can affect the risk of thrombosis in the medium and long term. Moreover, we have confirmed that the fact that a patient sleeps recurrently on her/his left/right side affects the flow split ratio and thus may modify the atrial flow patterns and the risk of stasis [47].

4.2. Limitations

Clinical images of two representative patients with AF were used for the study. Although a larger cohort will be necessary to confirm and generalize the results obtained, the morphing applied to the PV allowed to increase the number to 18 different geometries, which means a total number of 36 simulations (2 flow split ratios per geometry). We believe that this data-augmented cohort was large enough to meet the objective of the study, which was to analyze the influence of PV orientations on LAA washing, isolating the rest of the morphological and flow-related parameters.

The use of a kinematic atrial model allowed us to isolate the effect of local fibrotic patterns from the anatomical effects, facilitating comparison between different patient-specific geometries. Although we know that this limits the patient specificity of the models, which may not fully reflect the specific flow characteristics, it offers a useful modeling alternative [51, 52, 24] and its efficacy in replicating the LA and LAA hemodynamics was recently demonstrated [53]. In our case, it allowed for the isolation of geometrical and functional parameters and thus the study of the isolated effect of PV orientations on LAA blood stasis.

Similarly to most previous numerical studies of LA, an MV model was not considered [19, 32, 30, 22]. This assumption is justified by whole-left-heart simulations, which suggest that the dynamics of MV does not affect atrial flow patterns [21].

Biochemical modeling of thrombus formation was not included in our blood analysis. It would have required considering multiple biochemical equations [89, 90], increasing the computational burden. In addition, their precision is still limited due to the difficulty of adapting to patient-specific chemical reactions [47].

4.3. Conclusion

This study aimed to gain a more comprehensive understanding of the relationship between PV orientations and atrial flow patterns and its effect on blood stasis within the LAA. To this end, some of the most recent techniques in the field were applied: an atrial morphing process to analyze

the isolated effect of modifying the PV orientations, an atrial kinematic model to isolate anatomical from functional effects, and projection of the wall results on the ULAAC system to facilitate visualization and comparison of data between different cases. Special interest has been placed on studying the formation of the main atrial vortex and its interaction with RPV flow. The results show, with a systematic approach, how the position of the main atrial vortex can be significantly modified by changes in the LPV orientations. This, to the best of our knowledge, has not been done before. Moreover, the results also show how the RPV also play an important role, as their interaction with the main atrial vortex is crucial to define the LA patterns and, thus, the LAA washing. For the first time, we demonstrated how the flow patterns and their response to changes in the flow split ratio as a result of the patient's lying position can be totally changed by a combination of modifications in the LPV and RPV orientations, which therefore play a fundamental role in the quality of the LAA washing.

Acknowledgments

This work was supported by Junta de Extremadura and FEDER funds under project IB20105. We thank the Programa Propio - Universidad Politécnica de Madrid, and the Ayuda Primeros Proyectos de Investigación ETSII-UPM. We also thank Programa de Excelencia para el Profesorado Universitario de la Comunidad de Madrid for its financial support and the CeSViMa UPM project for its computational resources.

References

- [1] M. Stachyra, A. Glowinski, and E. Czekajka-Chehab. Atrial fibrillation ablation: the position of computed tomography in pre-procedural imaging. *Current Issues in Pharmacy and Medical Sciences*, 35:116–122, 2022.
- [2] M. Jiao, C. Liu, Y. Liu, Y. Wang, Q. Gao, and A. Ma. Estimates of the global, regional, and national burden of atrial fibrillation in older adults from 1990 to 2019: insights from the global burden of disease study 2019. *Front. Public Health*, 11:1137230, 2023.
- [3] G. Lippi, F. Sanchis-Gomar, and G. Cervellin. Global epidemiology of atrial fibrillation: An increasing epidemic and public health challenge. *Int. J. Stroke.*, 16:217–221, 2021.
- [4] E Szczepanek, F Bolechała, M Koziej, KA Jasińska, and MK Holda. Morphometric characteristics of myocardial sleeves of the pulmonary veins. *J Cardiovasc Electrophysiol.*, 31:2455–2461, 2020.
- [5] Patrick M Boyle, Juan Carlos Del Álamo, and Nazem Akoum. Fibrosis, atrial fibrillation and stroke: clinical updates and emerging mechanistic models. *Heart*, 107(2):99–105, 2021.
- [6] N. Fukui, T. Kanahashi, J. Matsubayashi, H. Imai, A. Yoneyama, H. Otani, S. Yamada, and T. Takakuwa. Morphogenesis of the pulmonary vein and left atrial appendage in human embryos and early fetuses. *J Anat.*, 244:142–158, 2024.
- [7] P. Rajiah, M. Alkhouli, J. Thaden, T. Foley, E. Williamson, and P. Ranganath. Pre- and postprocedural ct of transcatheter left atrial appendage closure devices. *RadioGraphics*, 41:680–698, 2021.
- [8] Florentino Lupercio, Juan Carlos Ruiz, David F Briceno, Jorge Romero, Pedro A Villablanca, Cecilia Berardi, Robert Faillace, Andrew Krumerman, John D Fisher, Kevin Ferrick, et al. Left atrial appendage morphology assessment for risk stratification of embolic stroke in patients with atrial fibrillation: a meta-analysis. *Heart Rhythm*, 13(7):1402–1409, 2016.

- [9] Brian D Hoit. Left atrial size and function: role in prognosis. *Journal of the American College of Cardiology*, 63(6):493–505, 2014.
- [10] Hooman Kamel, Peter M Okin, Mitchell SV Elkind, and Costantino Iadecola. Atrial fibrillation and mechanisms of stroke: time for a new model. *Stroke*, 47(3):895–900, 2016.
- [11] Philip A. Wolf, Robert D. Abbott, and William B. Kannel. Atrial fibrillation as an independent risk factor for stroke: The framingham study. *Stroke*, 22(8):983–988, 1991.
- [12] D. Gonzalez-Casal, T. Datino, N. Soto, T. González-Panizo, D. Sánchez-Quintana, Y. Macias, and J. A. Cabrera. Anatomy of the left atrial appendage for the interventional cardiologist. *Herzschr Elektrophys*, 33:195–202, 2022.
- [13] A.E. Darby. Recurrent atrial fibrillation after catheter ablation: Considerations for repeat ablation and strategies to optimize success. *J Atr Fibrillation*, 9:41–48, 2016.
- [14] Laurent Fauchier, Alexandre Cinaud, François Brigadeau, Antoine Lepillier, Bertrand Pierre, Selim Abbey, Marjaneh Fatemi, Frederic Franceschi, Paul Guedeny, Peggy Jacon, Olivier Paziud, Sandrine Venier, Jean Claude Deharo, Daniel Gras, Didier Klug, Jacques Mansourati, Gilles Montalescot, Olivier Piot, and Pascal Defaye. Device-Related Thrombosis After Percutaneous Left Atrial Appendage Occlusion for Atrial Fibrillation. *Journal of the American College of Cardiology*, 71(14):1528–1536, 2018.
- [15] Adel Aminian, Boris Schmidt, Patrizio Mazzone, Sergio Berti, Sven Fischer, Matteo Montorfano, Simon Cheung Chi Lam, Juha Lund, Federico M. Asch, Ryan Gage, Ignacio Cruz-Gonzalez, Heyder Omran, Giuseppe Tarantini, and Jens Erik Nielsen-Kudsk. Incidence, Characterization, and Clinical Impact of Device-Related Thrombus Following Left Atrial Appendage Occlusion in the Prospective Global AMPLATZER Amulet Observational Study. *JACC: Cardiovascular Interventions*, 12(11):1003–1014, 2019.
- [16] S. Valvez, M. Oliveira-Santos, A.P. Piedade, L. Gonçalves, and A.M. Amaro. Computational flow dynamic analysis in left atrial appendage thrombus formation risk: A review. *Appl. Sci.*, 13:8201, 2023.
- [17] J. Mill, J. Harrison, M. Saiz-Vivo, C. Albors, X. Morales, A. L. Olivares, X. Iriart, H. Cochet, J. Noailly, M. Sermesant, and O. Camara. The role of the pulmonary veins on left atrial flow patterns and thrombus formation. *Sci. Rep.*, 14:5860, 2024.
- [18] Christophe Chnafa, Simon Mendez, and Franck Nicoud. Image-based large-eddy simulation in a realistic left heart. *Computers & Fluids*, 94:173–187, 2014.
- [19] Tomohiro Otani, Abdullah Al-Issa, Amir Pourmorteza, Elliot R. McVeigh, Shigeo Wada, and Hiroshi Ashikaga. A Computational Framework for Personalized Blood Flow Analysis in the Human Left Atrium. *Annals of Biomedical Engineering*, 44(11):3284–3294, 2016.
- [20] Jonas Lantz, Vikas Gupta, Lilian Henriksson, Matts Karlsson, Anders Persson, Carl Johan Carlhäll, and Tino Ebbers. Impact of Pulmonary Venous Inflow on Cardiac Flow Simulations: Comparison with In Vivo 4D Flow MRI. *Annals of Biomedical Engineering*, 47(2):413–424, 2019.
- [21] Vijay Vedula, Richard George, Laurent Younes, and Rajat Mittal. Hemodynamics in the left atrium and its effect on ventricular flow patterns. *Journal of Biomechanical Engineering*, 137(11):1–8, 2015.
- [22] Michele Bucelli, Alberto Zingaro, Pasquale Claudio Africa, Ivan Fumagalli, Luca Dede', and Alfio Quarteroni. A mathematical model that integrates cardiac electrophysiology, mechanics and fluid dynamics: application to the human left heart. *International Journal for Numerical Methods in Biomedical Engineering*, page e3678, 2022.
- [23] Viorel Mihalef, Razvan Ioan Ionasec, Puneet Sharma, Bogdan Georgescu, Ingmar Voigt, Michael Sueling, and Dorin Comaniciu. Patient-specific modelling of whole heart anatomy, dynamics and haemodynamics from four-dimensional cardiac ct images. *Interface Focus*, 1(3):286–296, 2011.
- [24] Mattia Corti, Alberto Zingaro, Alfio Maria Quarteroni, et al. Impact of atrial fibrillation on left atrium haemodynamics: A computational fluid dynamics study. *Computers in Biology and Medicine*, 150:106143, 2022.
- [25] Alejandro Gonzalo, Manuel García-Villalba, Lorenzo Rossini, Eduardo Durán, Davis Vigneault, Pablo Martínez-Legazpi, Oscar Flores, Javier Bermejo, Elliot McVeigh, Andrew M Kahn, et al. Non-newtonian blood rheology impacts left atrial stasis in patient-specific simulations. *International Journal for Numerical Methods in Biomedical Engineering*, 38(6):e3597, 2022.
- [26] Liuyang Feng, Hao Gao, Boyce Griffith, Steven Niederer, and Xiaoyu Luo. Analysis of a coupled fluid-structure interaction model of the left atrium and mitral valve. *International journal for numerical methods in biomedical engineering*, 35(11):e3254, 2019.
- [27] Giorgia Maria Bosi, Andrew Cook, Rajan Rai, Leon J. Menezes, Silvia Schievano, Ryo Torii, and Gaetano Burriesci. Computational Fluid Dynamic Analysis of the Left Atrial Appendage to Predict Thrombosis Risk. *Frontiers in Cardiovascular Medicine*, 5(April):1–8, 2018.
- [28] Guadalupe García-Isla, Andy Luis Olivares, Etelvino Silva, Marta Nuñez-García, Constantine Butakoff, Damian Sanchez-Quintana, Hernán G. Morales, Xavier Freixa, Jérôme Noailly, Tom De Potter, and Oscar Camara. Sensitivity analysis of geometrical parameters to study haemodynamics and thrombus formation in the left atrial appendage. *International Journal for Numerical Methods in Biomedical Engineering*, 34(8):1–14, 2018.
- [29] Alessandro Masci, Lorenzo Barone, Luca Dedè, Marco Fedele, Corrado Tomasi, Alfio Quarteroni, and Cristiana Corsi. The impact of left atrium appendage morphology on stroke risk assessment in atrial fibrillation: A computational fluid dynamics study. *Frontiers in Physiology*, 9(January):1–11, 2019.
- [30] Jorge Dueñas-Pamplona, Javier García García, Jose Sierra-Pallares, Conrado Ferrera, Rafael Agujetas, and Jose Ramon Lopez-Minguez. A comprehensive comparison of various patient-specific cfd models of the left atrium for atrial fibrillation patients. *Computers in Biology and Medicine*, 133:104423, 2021.
- [31] Ryo Koizumi, Kenichi Funamoto, Toshiyuki Hayase, Yusuke Kanke, Muneichi Shibata, Yasuyuki Shiraiishi, and Tomoyuki Yambe. Numerical analysis of hemodynamic changes in the left atrium due to atrial fibrillation. *Journal of Biomechanics*, 48(3):472–478, 2015.
- [32] Manuel García-Villalba, Lorenzo Rossini, Alejandro Gonzalo, Davis Vigneault, Pablo Martínez-Legazpi, Eduardo Durán, Oscar Flores, Javier Bermejo, Elliot McVeigh, Andrew M Kahn, et al. Demonstration of patient-specific simulations to assess left atrial appendage thrombogenesis risk. *Frontiers in physiology*, 12:596596, 2021.
- [33] Eduardo Durán, Manuel García-Villalba, Pablo Martínez-Legazpi, Alejandro Gonzalo, Elliot McVeigh, Andrew M Kahn, Javier Bermejo, Oscar Flores, and Juan Carlos Del Álamo. Pulmonary vein flow split effects in patient-specific simulations of left atrial flow. *Computers in Biology and Medicine*, page 107128, 2023.
- [34] Luigi Di Biase, Pasquale Santangeli, Matteo Anselmino, Prasant Mohanty, Ilaria Salvetti, Sebastiano Gili, Rodney Horton, Javier E. Sanchez, Rong Bai, Sanghamitra Mohanty, Agnes Pump, Mauricio Cereceda Brantes, G. Joseph Gallinghouse, J. David Burkhardt, Federico Cesarani, Marco Scaglione, Andrea Natale, and Fiorenzo Gaita. Does the left atrial appendage morphology correlate with the risk of stroke in patients with atrial fibrillation? Results from a multicenter study. *Journal of the American College of Cardiology*, 60(6):531–538, 2012.
- [35] Masayoshi Yamamoto, Yoshihiro Seo, Naoto Kawamatsu, Kimi Sato, Akinori Sugano, Tomoko Machino-Ohtsuka, Ryo Kawamura, Hideki Nakajima, Miyako Igarashi, Yukio Sekiguchi, et al. Complex left atrial appendage morphology and left atrial appendage thrombus formation in patients with atrial fibrillation. *Circulation: Cardiovascular Imaging*, 7(2):337–343, 2014.
- [36] Jorge Dueñas-Pamplona, Javier Garcia Garcia, Francisco Castro, Jorge Munoz-Paniagua, Javier Goicolea, and Jose Sierra-Pallares. Morphing the left atrium geometry: A deeper insight into blood stasis within the left atrial appendage. *Applied Mathematical Modelling*, 108:27–45, 2022.
- [37] P Di Achille, G Tellides, CA Figueroa, and JD Humphrey. A haemodynamic predictor of intraluminal thrombus formation in abdominal

- aortic aneurysms. *Proceedings of the Royal Society A: Mathematical, Physical and Engineering Sciences*, 470(2172):20140163, 2014.
- [38] Yan Wang, Luigi Di Biase, Rodney P. Horton, Tuan Nguyen, Prasant Morhanty, and Andrea Natale. Left atrial appendage studied by computed tomography to help planning for appendage closure device placement. *Journal of Cardiovascular Electrophysiology*, 21(9):973–982, 2010.
- [39] Shadi Yaghi, Andrew D Chang, Ronald Akiki, Scott Collins, Tracy Novack, Morgan Hemendinger, Ashley Schomer, Brain Mac Grory, Shawna Cutting, Tina Burton, et al. The left atrial appendage morphology is associated with embolic stroke subtypes using a simple classification system: a proof of concept study. *Journal of cardiovascular computed tomography*, 14(1):27–33, 2020.
- [40] Woo Kyo Jeong, Jin Ho Choi, Jeong Pyo Son, Suyeon Lee, Mi Ji Lee, Yeon Hyeon Choe, and Oh Young Bang. Volume and morphology of left atrial appendage as determinants of stroke subtype in patients with atrial fibrillation. *Heart Rhythm*, 13(4):820–827, 2016.
- [41] Maria Isabel Pons, Jordi Mill, Alvaro Fernandez-Quilez, Andy L Olivares, Etelvino Silva, Tom De Potter, Oscar Camara, et al. Joint analysis of morphological parameters and in silico haemodynamics of the left atrial appendage for thrombotic risk assessment. *Journal of Interventional Cardiology*, 2022, 2022.
- [42] Roy Beinart, E Kevin Heist, John B Newell, Godtfred Holmvang, Jeremy N Ruskin, and Moussa Mansour. Left atrial appendage dimensions predict the risk of stroke/tia in patients with atrial fibrillation. *Journal of cardiovascular electrophysiology*, 22(1):10–15, 2011.
- [43] Jung Myung Lee, Jin-Bae Kim, Jae-Sun Uhm, Hui-Nam Pak, Moon-Hyoung Lee, and Boyoung Joung. Additional value of left atrial appendage geometry and hemodynamics when considering anticoagulation strategy in patients with atrial fibrillation with low cha2ds2-vasc scores. *Heart Rhythm*, 14(9):1297–1301, 2017.
- [44] J. Mill, V. Agudelo, A. L. Olivares, M. I. Pons, E. Silva, M. Nuñez-García, Morales X., D. Arzamendi, X. Freixa, J. Noailly, and O. Camara. Sensitivity analysis of in silico fluid simulations to predict thrombus formation after left atrial appendage occlusion. *Mathematics*, 9:2304, 2021.
- [45] Jorge Dueñas-Pamplona, Sergio Rodríguez-Aparicio, Alejandro Gonzalo, Savannah F Bifulco, Francisco Castro, Conrado Ferrera, Óscar Flores, Patrick M Boyle, José Sierra-Pallares, Javier García García, et al. Reduced-order models of wall shear stress patterns in the left atrial appendage from a data-augmented atrial database. *Applied Mathematical Modelling*, 130:713–727, 2024.
- [46] Jorge Dueñas-Pamplona, José Sierra-Pallares, Javier García, Francisco Castro, and Jorge Munoz-Paniagua. Boundary-condition analysis of an idealized left atrium model. *Annals of Biomedical Engineering*, 49(6):1507–1520, 2021.
- [47] S. Rodríguez-Aparicio, C. Ferrera, M. V. Millán-Núñez, J. García-García, and J. Dueñas-Pamplona. Influence of the flow split ratio on the position of the main atrial vortex: Implications for stasis on the left atrial appendage. *Computers in Biology and Medicine*, 178:108772, 2024.
- [48] Lucy T Zhang and Mickael Gay. Characterizing left atrial appendage functions in sinus rhythm and atrial fibrillation using computational models. *Journal of biomechanics*, 41(11):2515–2523, 2008.
- [49] O. Hazan, L. Sternik, D. Waiss, M. Eldar, O. Hoffer, O. Goitein, R. Kuperstein, E. Konen, and Z. Ovadia-Blechman. An innovative appendage invagination procedure to reduce thrombus formation in a numerical model. *Computer Methods in Biomechanics and Biomedical Engineering*, 21(4):370–378, 2018.
- [50] Xabier Morales Ferez, Jordi Mill, Kristine Aavild Juhl, Cesar Acebes, Xavier Iriart, Benoit Legghe, Hubert Cochet, Ole De Backer, Rasmus R Paulsen, and Oscar Camara. Deep learning framework for real-time estimation of in-silico thrombotic risk indices in the left atrial appendage. *Frontiers in Physiology*, 12:694945, 2021.
- [51] Alberto Zingaro, Ivan Fumagalli, Luca Dede, Marco Fedele, Pasquale Claudio Africa, Antonio Francesco Corno, and Alfio Quarteroni. A geometric multiscale model for the numerical simulation of blood flow in the human left heart, 2022.
- [52] Alberto Zingaro, Luca Dede, Filippo Menghini, and Alfio Quarteroni. Hemodynamics of the heart’s left atrium based on a variational multiscale-les numerical method. *European Journal of Mechanics - B/Fluids*, 89:380–400, 2021.
- [53] Henrik A Kjeldsberg, Carlos Albors, Jordi Mill, David Viladés Medel, Oscar Camara, Joakim Sundnes, and Kristian Valen-Sendstad. Impact of left atrial wall motion assumptions in fluid simulations on proposed predictors of thrombus formation. *International Journal for Numerical Methods in Biomedical Engineering*, page e3825, 2024.
- [54] A. Masci, M. Alessandrini, L. Dede, D. Forti, F. Menghini, C. Tomasi, A. Quarteroni, and C. Corsi. Development of a computational fluid dynamics model of the left atrium in atrial fibrillation on a patient specific basis. In *44th Computing in Cardiology Conference, CinC 2017*, pages 1–4, 2017.
- [55] E. M. Marom, J. E. Herndon, Y. H. Kim, and H. P. McAdams. Variations in pulmonary venous drainage to the left atrium: Implications for radiofrequency ablation. *Radiology*, 230(3):824–829, 2004.
- [56] J. Mill, J. Harrison, B. Legghe, A. L. Olivares, X. Morales, J. Noailly, X. Iriart, H. Cochet, M. Sermesant, and O. Camara. In-silico analysis of the influence of pulmonary vein configuration on left atrial haemodynamics and thrombus formation in a large cohort. In D. B. Ennis, L. E. Perotti, and V. Y. Wang, editors, *Functional Imaging and Modeling of the Heart*, pages 605–616, Cham, 2021. Springer International Publishing.
- [57] Mateusz Polaczek, Pawel Szaro, Inga Baranska, Barbara Burakowska, and Bogdan Ciszek. Morphology and morphometry of pulmonary veins and the left atrium in multi-slice computed tomography. *Surgical and Radiologic Anatomy*, 41(7):721–730, 2019.
- [58] Runxin Fang, Zidun Wang, Xie Zhao, Jun Wang, Yang Li, Yanjuan Zhang, Qiang Chen, Jiaqiu Wang, Quanjun Liu, Minglong Chen, and Zhiyong Li. Stroke risk evaluation for patients with atrial fibrillation: Insights from left atrial appendage with fluid-structure interaction analysis. *Computers in Biology and Medicine*, 148:105897, 2022.
- [59] S.K. Dahl, E. Thomassen, L. R Hellevik, and B. Skallerud. Impact of pulmonary venous locations on the intra-atrial flow and the mitral valve plane velocity profile. *Cardiovascular Engineering and Technology*, 3:269–281, 2012.
- [60] R. Fang, Y. Li, Y. Zhang, Q. Chen, Q. Liu, and Li Z. Impact of left atrial appendage location on risk of thrombus formation in patients with atrial fibrillation. *Biomech Model Mechanobiol*, 20:1431–1443, 2021.
- [61] N. Szegedi, M. Vecsey-Nagy, J. Simon, B. Szilveszter, S. Herczeg, M. Kolossváry, H. Idelbi, I. Osztheimer, V.K. Nagy, T. Tahin, G. Széplaki, V. Delgado, J. J. Bax, P. Maurovich-Horvat, B. Merkely, and L. Gellér. Orientation of the right superior pulmonary vein affects outcome after pulmonary vein isolation. *European Heart Journal - Cardiovascular Imaging*, 23(4):515–523, 2021.
- [62] P. Gal, J.F.W. Ooms, J. P. Ottervanger, J. J. J. Smit, A. Adiyaman, Anand R. Ramdat M., P.P.H.M. Delnoy, P.L. Jager, and A. Elvan. Association between pulmonary vein orientation and atrial fibrillation-free survival in patients undergoing endoscopic laser balloon ablation. *European Heart Journal - Cardiovascular Imaging*, 16(7):799–806, 2015.
- [63] P. Gal, T.J. Buist, J.J.J.T. Smit, A. Adiyaman, A. R. Ramdat Misier, and A. et al. Delnoy, P. P. H. M. and Elvan. Effective contact and outcome after pulmonary vein isolation in novel circular multi-electrode atrial fibrillation ablation. *Neth. Heart J.*, 25:16–23, 2017.
- [64] Blender Documentation Team. *Blender 3.6 Reference Manual*. Blender Foundation, Blender Institute B.V., Amsterdam, 2023.
- [65] Keenan Crane, Clarisse Weischedel, and Max Wardetzky. The heat method for distance computation. *Communications of the ACM*, 60(11):90–99, 2017.
- [66] R B. Bird, R. C. Armstrong, and O. Hassager. *Dynamic of Polymer Liquids*. John Wiley, 1987.
- [67] Y. I. Cho and K. R Kensey. Effects of the non-newtonian viscosity of blood on flows in a diseased arterial vessel. part 1: Steady flows. *Biorheology*, 28:241–262, 1991.

- [68] José Sierra-Pallares, César Méndez, Pedro García-Carrascal, and Francisco Castro. Spatial distribution of mean age and higher moments of unsteady and reactive tracers: Reconstruction of residence time distributions. *Applied Mathematical Modelling*, 46:312–327, 2017.
- [69] Caterina Balzotti, Pierfrancesco Siena, Michele Girfoglio, Giovanni Stabile, Jorge Dueñas-Pamplona, José Sierra-Pallares, Ignacio Amats-Santos, and Gianluigi Rozza. A reduced order model formulation for left atrium flow: an atrial fibrillation case. *arXiv preprint arXiv:2309.10601*, 2023.
- [70] Jeng-Jiann Chiu and Shu Chien. Effects of disturbed flow on vascular endothelium: pathophysiological basis and clinical perspectives. *Physiological reviews*, 91(1):327–387, 2011.
- [71] Caroline H Roney, Ali Pashaei, Marianna Meo, Rémi Dubois, Patrick M Boyle, Natalia A Trayanova, Hubert Cochet, Steven A Niederer, and Edward J Vigmond. Universal atrial coordinates applied to visualisation, registration and construction of patient specific meshes. *Medical image analysis*, 55:65–75, 2019.
- [72] Jason Bayer, Anton J Prassl, Ali Pashaei, Juan F Gomez, Antonio Frontera, Aurel Neic, Gernot Plank, and Edward J Vigmond. Universal ventricular coordinates: A generic framework for describing position within the heart and transferring data. *Medical image analysis*, 45:83–93, 2018.
- [73] Martin Reuter, Franz-Erich Wolter, and Niklas Peinecke. Laplace–Beltrami spectra as ‘shape-dna’ of surfaces and solids. *Computer-Aided Design*, 38(4):342–366, 2006.
- [74] Christian Wachinger, Polina Golland, William Kremen, Bruce Fischl, Martin Reuter, Alzheimer’s Disease Neuroimaging Initiative, et al. Brainprint: A discriminative characterization of brain morphology. *NeuroImage*, 109:232–248, 2015.
- [75] E. Khalili, C. Daversin-Catty, A. L. Olivares, J. Mill, O. Camara, and K. Valen-Sendstad. On the importance of fundamental computational fluid dynamics toward a robust and reliable model of left atrial flows. *International Journal for Numerical Methods in Biomedical Engineering*, 40:e3804, 2024.
- [76] Tsutomu Takagi, Atsushi Takagi, and Junichi Yoshikawa. Altered trans-mitral flow velocity pattern after exercise predicts development of new-onset atrial fibrillation in elderly patients with impaired left ventricular relaxation at rest: Prognostic value of diastolic stress echocardiography. *Journal of Cardiology*, 59(2):225–234, 2012.
- [77] Gerardo E. Farese, Bhupendar Tayal, Stephan Stöbe, Ulrich Laufs, and Andreas Hagendorff. Regional disparities of left atrial appendage wall contraction in patients with sinus rhythm and atrial fibrillation. *Journal of the American Society of Echocardiography*, 32(6):755–762, 2019.
- [78] Adrian D. Elliott, Jonathan Ariyaratnam, Erin J. Howden, Andre La Gerche, and Prashanthan Sanders. Influence of exercise training on the left atrium: implications for atrial fibrillation, heart failure, and stroke. *American Journal of Physiology-Heart and Circulatory Physiology*, 325(4):H822–H836, 2023.
- [79] B. Wieslander, J. Ramos, M. Ax, J. Petersson, and M. Ugander. Supine, prone, right and left gravitational effects on human pulmonary circulation. *J. Cardiovasc. Magn. Reson.*, 21(69), 2019.
- [80] C. Albers, A. L. Olivares, X. Iriart, H. Cochet, J. Mill, and O. Camara. Impact of blood rheological strategies on the optimization of patient-specific laao configurations for thrombus assessment. In O. Bernard, P. Clarysse, N. Duchateau, J. Ohayon, and M. Viallon, editors, *Functional Imaging and Modeling of the Heart*, volume 13958 of *Lecture Notes in Computer Science*, pages 485–494, Cham, June 2023. Springer Nature Switzerland.
- [81] R. Agujetas, M. R. González-Fernández, J. M. Nogales-Asensio, and J. M. Montanero. Numerical analysis of the pressure drop across highly-eccentric coronary stenoses: application to the calculation of the fractional flow reserve. *Biomed. Eng. OnLine*, 17:67, 2018.
- [82] Jordi Mill, Andy L. Olivares, Dabit Arzamendi, Victor Agudelo, Ander Regueiro, Oscar Camara, and Xavier Freixa. Impact of Flow Dynamics on Device-Related Thrombosis After Left Atrial Appendage Occlusion. *Canadian Journal of Cardiology*, 36(6):968.e13–968.e14, 2020.
- [83] Vijay Vedula, Jung-Hee Seo, Albert C Lardo, and Rajat Mittal. Effect of trabeculae and papillary muscles on the hemodynamics of the left ventricle. *Theoretical and Computational Fluid Dynamics*, 30:3–21, 2016.
- [84] J. C. R. Hunt, A. A. Wray, and P. Moin. Eddies, stream, and convergence zones in turbulent flows. In *Proceedings of the Summer Program (Center for Turbulence Research Report)*, pages 193–208. Stanford University, July 1988.
- [85] J. Jeong and F. Hussain. On the identification of a vortex. *Journal of Fluid Mechanics*, 285:69–94, 1995.
- [86] Yanlu Chen, Buyun Xu, Yuzhou Cheng, Kun Luo, Jianren Fan, and Meixiang Xiang. Hemodynamic differences caused by left atrial appendage modeling contours. *Physics of Fluids*, 35(11), 2023.
- [87] G. Rigatelli, M. Zuin, S. Agarwal, V. Nguyen, C. Nguyen, S. Agarwal, and T. Nguyen. Applications of computational fluid dynamics in cardiovascular disease. *J. Biomed. Sci.*, 1:12–20, 2022.
- [88] P.D. Morris, A. Narracott, H. von Teng-Kobligk, et al. Computational fluid dynamics modelling in cardiovascular medicine. *Heart*, 102:18–28, 2016.
- [89] Jung Hee Seo, Thura Abd, Richard T George, and Rajat Mittal. A coupled chemo-fluidic computational model for thrombogenesis in infarcted left ventricles. *American Journal of Physiology-Heart and Circulatory Physiology*, 310(11):H1567–H1582, 2016.
- [90] R. Méndez-Rojano, S. Mendez, and F. Nicoud. Introducing the pro-coagulant contact system in the numerical assessment of device-related thrombosis. *Biomech. Model. Mechanobiol.*, 17:815–826, 2018.